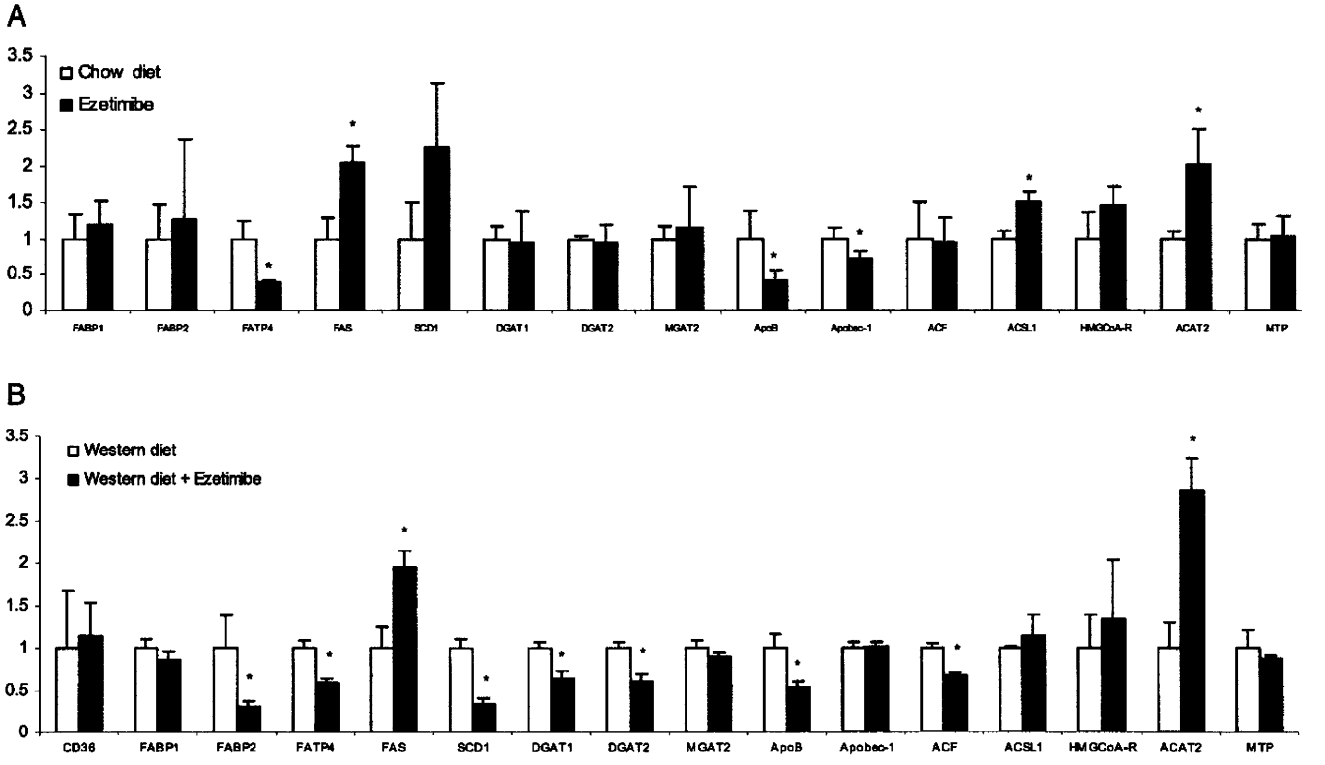

Fig. 5. Effect of Ezetimibe on the Transcriptional Regulation of Genes Involved in Fatty Acid Transport, TG Formation and CM Assembly in the Intestinal Cells in the Postprandial State.

We performed qRT-PCR using total mRNA isolated from intestines, and examined the expression of genes associated with FA transport, TG formation and CM assembly for CD36KO (A) and found that ezetimibe administration significantly inhibited the expression of FATP4, apoB and apobec1. In WT mice (B) ezetimibe decreased the expression of FATP4, FABP2, DGAT1, DGAT2, SCD1, apoB and ACF significantly. There was also the upregulation of FAS and ACAT2, which could correspond to a compensatory response. In both cases, ezetimibe decreased the expression of genes involved in FA metabolism and CM production.

genic model of MetS[11]. We have elucidated the possible molecular mechanisms responsible for the reduced production of ApoB-48-containing lipoproteins in intestinal epithelial cells. Because of the lack of hepatic NPC1L1 expression in mice[20], the usage of mice has an advantage to understanding the physiological mechanisms of lipid metabolism in the small intestines as a main target of ezetimibe, contrary to human subjects in which NPC1L1 is believed to be expressed in both small intestines and the liver. Ezetimibe is a strong inhibitor of cholesterol absorption via NPC1L1, and thus cholesterol incorporation into the CM synthesized in the small intestines is reduced by ezetimibe treatment. Therefore, the reduction of cholesterol content in CM and CM remnants may result in a decreased cholesterol pool in the liver, leading to the enhancement of hepatic LDL receptor. Thus, ezetimibe treatment may enhance the catabolism of LDL via hepatic LDL receptor, resulting in the reduction of LDL-cholesterol and possibly CM remnants. Furthermore, reduced cholesterol absorption may lead to the loss of the substrate for CM formation and thereby to attenuation of CM synthesis in the small intestines.

We found that, in both groups, WT mice fed a high fat diet and CD36KO mice fed a chow diet, ezetimibe did not reduce plasma cholesterol concentrations significantly in the fasting state (**Fig. 1B**); however, there remained a small, non-significant tendency for the cholesterol content in plasma to fall in both groups. This might be associated with increased endogenous production of cholesterol in both the intestine and liver in both models, possibly through an increased expression of HMG-CoA synthase, which should be further considered.

We also found that in WT mice fed a chow diet, ezetimibe did not decrease postprandial TG levels (**Fig. 1A**); however, when WT mice were fed a high-fat, high-cholesterol diet, ezetimibe reduced the PHTG to normal levels. This might suggest that ezetimibe could reduce postprandial triglyceride levels in

conditions of CM overproduction.

In a previous publication, our group found that CD36KO mice have an increased TG response to acute fat loads in both plasma and lymph[11]. In the current study, we found that CD36KO showed a higher TG concentration than WT mice even in a high fat loading state in intestinal lymph (**Fig. 3**); this might suggest the hypothesis that CD36KO mice would have a larger CM than WT mice. However, since the CM fraction in our HPLC method was included in the void volume, we could not determine the specific size of individual particles in this fraction, which is considered a whole group, and therefore, we were not able to confirm whether there was really a difference in particle size between these two groups.

The reduced absorption of long-chain FAs observed in this study was in part associated with an inhibitory effect on FATP4 in CD36KO mice as well as the reduction of both FATP4 and FABP2 intestinal expression in WT mice. FATP4 is the only FATP expressed in the intestines[21], is located in the ER of the intestinal cells and has demonstrated acyl-CoA synthetase activity, which decreases the intracellular concentration of FAs, and would indirectly increase FA uptake when the extracellular concentration is high enough, as in the postprandial state[22]. FATP4 has also been associated with obesity and the insulin-resistant state[23]. Labonté *et al.*[24] reported a reduction of the FATP4 amount in the intestines of both WT mice receiving ezetimibe and NPC1L1 knockout mice compared to WT controls. Although we did not measure the amount of FATP4 protein by Western blotting, we found a decrease in the mRNA content in both treated groups, suggesting inhibition of the regulation of FATP4 at the transcriptional level, which would lead to a decreased amount of FATP4. Taken together, these findings suggest a close relationship between the presence of active NPC1L1 and the uptake, intracellular transport and esterification of long-chain FAs.

In the current study, we also found that WT mice fed a western diet under ezetimibe treatment showed a reduced expression of DGAT1 and DGAT2, two proteins involved in TG synthesis, located in the ER[25], as well as a decreased expression of SCD1, which is an important lipogenic factor associated with dietary saturated fat-related obesity[26]. SCD1 has been reported to colocalize and interact with DGAT2[27], suggesting a mechanism of the incorporation of endogenously synthesized FAs into TG. Therefore, ezetimibe might also decrease PHTG in WT mice fed a western diet by reducing the formation of TG in intestinal cells.

Interestingly, in CD36KO mice, ezetimibe administration inhibited only FATP4 expression in the steps prior to CM assembly to reduce PHTG, but not FABP2, nor any of the proteins involved in TG production, as in WT mice, which might suggest that FATP4 could play an essential role in FA metabolism in the CD36KO model, different from WT mice, which also supports the idea that intestinal lipid metabolism in CD36KO mice is different from in WT mice.

On the other hand, we found that ezetimibe administration reduced ApoB mRNA in both treated groups, and moreover, ezetimibe decreased the mRNA levels of apobec1 in CD36KO mice and Apobec1 complementary factor (ACF) in WT mice. Whether ezetimibe decreased ApoB48 mass in lymph only by inhibiting the transcription or by enhancing the post-transcriptional degradation of ApoB is not known yet, and further examination will be required to gain a better understanding of intestinal ApoB metabolism.

Apobec1 is the catalytic subunit of the ApoB editing complex; in the absence of apobec1, there is no ApoB mRNA edition; apobec1 KO mice lack ApoB48, and the only ApoB found in this model is ApoB100[28]. In our study, ezetimibe decreased apobec1 mRNA significantly in CD36KO mice; however, we did not find any traces of ApoB100 in the intestinal lymph collected; therefore, we presume that ApoB mRNA edition was not so low as to make the enterocytes produce ApoB100-containing lipoproteins, but decreased enough to reduce the production of ApoB48 which, in addition to the presence of low TG as a substrate, led to reduced CM production.

Apobec1 complementary factor (ACF), the RNA-binding subunit of the editing complex, interacts with both apobec1 and ApoB mRNA, positioning the ApoB mRNA structure in the optimal configuration to expose the C residue to apobec1, and it has been proposed to be responsible for the specificity of the reaction[29], and a stabilizer for apobec1[30]. It has been proposed that ACF plays a pivotal role independent of apobec1, since attempts to generate ACF KO mice were not successful beyond the blastocyst state, and siRNA knockdown of ACF in rat and human cells induced an increase in apoptosis. In heterozygote ACF KO mice, ACF protein was found to be decreased in the small intestines; however, intestinal ApoB mRNA edition was not compromised[31]. From this evidence, we could not draw the conclusion that the lowering effect of ezetimibe on the expression of ACF would be actually relevant to ApoB mRNA edition and the production of CM in WT mice.

We have summarized in **Fig. 6** the possible

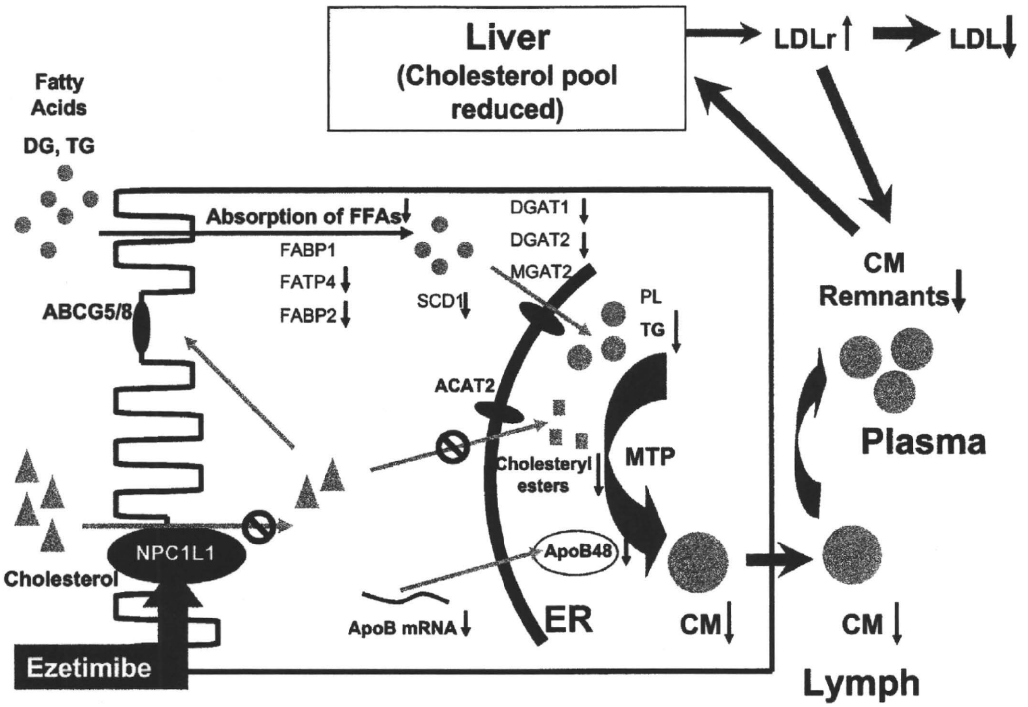

Fig. 6. Possible Mechanisms for the Inhibitory Effect of Ezetimibe on Postprandial Hypertriglyceridemia.

Administration of ezetimibe alone reduces PHTG by inhibiting cholesterol absorption and the expression of genes involved in the uptake, intracellular trafficking and metabolism of long-chain FAs (FATP4 in both WT and CD36KO mice and FABP2 in WT mice only), as well as by decreasing the formation of TG (SCD1, DGAT1 and DGAT2 in WT mice) and the expression of apoB (both WT and CD36KO mice), necessary for the production of ApoB48-containing lipoproteins in the small intestine. Furthermore, reduced cholesterol influx to the liver may lead to the up-regulation of hepatic LDL receptor, resulting in the enhanced catabolism of LDL and CM remnants.

mechanisms for the inhibitory effect of ezetimibe treatment on postprandial hypertriglyceridemia. The administration of ezetimibe alone reduces PHTG by inhibiting cholesterol absorption and the expression of genes involved in the uptake, intracellular trafficking and the metabolism of long-chain FAs (FATP4 in both WT and CD36KO mice and FABP2 in WT mice only), as well as by decreasing the formation of TG (SCD1, DGAT1 and DGAT2 in WT mice) and the expression of ApoB (both WT and CD36KO mice) necessary for the production of ApoB48-containing lipoproteins in the small intestine. Furthermore, reduced cholesterol influx to the liver may lead to the up-regulation of hepatic LDL receptor, resulting in the enhanced catabolism of LDL and CM remnants.

In conclusion, ezetimibe alone reduces PHTG in mouse models of MetS by inhibiting cholesterol absorption and uptake, intracellular trafficking and the metabolism of long-chain FAs, as well as decreasing the formation of TG and the expression of apoB, necessary for the production of apoB48-containing lipoproteins in the small intestine. Thus, ezetimibe strongly attenuates the intestinal production of CM, resulting in the inhibition of PHTG, which may eventually lead to the reduction of atherosclerosis in both animal models and humans.

Acknowledgments

This work was supported by the following grants: a grant-in-aid for Scientific Research (No. 18659267) to S. Yamashita from the Ministry of Education, Science, Sports and Culture in Japan; a grant from Mitsui Life Social Welfare Foundation to S. Yamashita; a Takeda Medical Research Foundation Grant to S. Yamashita.

References

1) Third Report of the National Cholesterol Education Program (NCEP): Expert Panel on Detection, Evaluation and Treatment of High Blood cholesterol in Adults (Adult treatment panel Ⅲ). Final Report. Circulation, 2002;

106: 3163-3223
2) Nordestgaard B, Benn M, Schnohr P, Tybjærg-Hansen A: Nonfasting triglycerides and risk of myocardial infarction, ischemic heart disease, and death in men and women. JAMA, 2007; 298: 299-308
3) Freiberg JJ, Tybjaerg-Hansen A, Jensen JS, Nordestgaard BG: Nonfasting triglycerides and risk of ischemic stroke in the general population. JAMA, 2008; 300: 2142-2152
4) Huff MW: Dietary cholesterol, cholesterol absorption, postprandial lipemia and aterosclerosis. Can J Clin Pharmacol, 2003; 10 (Suppl A): 26A-32A
5) Zilversmit DB: Atherogenesis: A postprandial phenomenon. Circulation, 1979; 60: 473-485
6) Fujioka Y, Ishikawa Y: Remnant lipoproteins as strong key particles to atherogenesis. J Atheroscler Thromb, 2009; 16: 145-154
7) Tanaka A: Postprandial hypertriglyceridemia and atherosclerosis. J Atheroscler Thromb, 2004; 11: 322-329
8) Su X, Abumrad NA: Cellular fatty acid uptake: A pathway under construction. Trends Endocrinol Metab, 2009; 20: 72-77
9) Yamashita S, Hirano K, Kuwasako T, Janabi M, Toyama Y, Ishigami M, Sakai N: Physiological and pathological roles of a multi-ligand receptor CD36 in atherogenesis; insights from CD36-deficient patients. Mol Cell Biochem, 2007; 299: 19-22
10) Goudriaan JR, den Boer MA, Rensen PC, Febbraio M, Kuipers F, Romijn JA, Havekes LM, Voshol PJ: CD36 deficiency in mice impairs lipoprotein lipase-mediated triglycerides clearance. J Lipid Res, 2005; 46: 2175-2181
11) Masuda D, Hirano K, Oku H, Sandoval JC, Kawase R, Yuasa-Kawase M, Yamashita Y, Takada M, Tsubakio-Yamamoto K, Tochino Y, Koseki M, Matsuura F, Nishida M, Kawamoto T, Ishigami M, Hori M, Shimomura I, Yamashita S: Chylomicron remnants are increased in the postprandial state in CD36 deficiency. J Lipid Res, 2009; 50: 999-1011
12) Ge L, Wang J, Qi W, Miao HH, Cao J, Qu YX, Li BL, Song BL: The cholesterol absorption inhibitor ezetimibe acts by blocking the sterol-induced internalization of NPC1L1. Cell Metab, 2008; 7: 508-519
13) Stein E, Stender S, Mata P, Sager P, Ponsonnet D, Melani L, Lipka L, Suresh R, MacCcubin D, Veltri E: Achieving lipoprotein goals in patients at high risk with severe hypercholesterolemia: Efficacy and safety of ezetimibe co-administered with atorvastatin. Am Heart J, 2004; 148: 447-455
14) McKenney JM, Farnier M, Lo KW, Bays HE, Perevozkaya I, Carlson G, Davies MJ, Mitchel YB, Gumbiner B: Safety and efficacy of long-term co-administration of fenofibrate and ezetimibe in patients with mixed hyperlipidemia. J Am Coll Cardiol, 2006; 47: 1584-1587
15) Hajer GR, Dallinga-Thie GM, van Vark-van der Zee LC, Visseren FL: The effect of statin alone or in combination with ezetimibe on postprandial lipoprotein composition in obese metabolic syndrome patients. Atherosclerosis, 2009; 202: 216-224
16) Masuda D, Nakagawa-Toyama Y, Nakatani K, Inagaki M, Tsubakio-Yamamoto K, Sandoval JC, Ohama T, Nishida M, Ishigami M, Yamashita S: Ezetimibe improves postprandial hyperlipidaemia in patients with type IIb hyperlipidaemia. Eur J Clin Invest, 2009; 39: 689-698
17) Moore KJ, J El Khoury J, Medeiros LA, Terada K, Geula C, Luster AD, Freeman MW: A CD36-initiated signaling cascade mediates inflammatory effects of beta-amyloid. J Biol Chem, 2002; 277: 47373-47379
18) Okazaki M, Usui S, Fukui A, Kubota I, Tomoike H: Component analysis of HPLC profiles of unique lipoprotein subclass cholesterols for detection of coronary artery disease. Clin Chem, 2006; 52: 2049-2053
19) Bollman, JL, Cain JC, Grindlay JH: Techniques for the collection of lymph from the liver, small intestine, or thoracic duct of the rat. J Lab Clin Med, 1949; 33: 1349-1352
20) Altmann SW, Davis HR, Zhu LJ, Yao X, Hoos LM, Tezloff G, Iyer SPN, Maguire M, Golovko A, Zeng M, Wang L, Murgolo N, Graziano MP: Niemann-Pick C1 Like 1 protein is critical for intestinal cholesterol absorption. Science, 2004; 303: 1201-1204
21) Stahl A: A current review of fatty acid transport proteins (SLC27). Pflugers Arch, 2004; 447: 722-727
22) Milger K, Herrmann T, Becker C, Gotthardt D, Zickwolf J, Ehehait R, Watkins P, Stremmel W, Füllekrug J: Cellular uptake of fatty acids driven by the ER-localized acyl-CoA synthetase FATP4. J Cell Sci, 2006; 119: 4678-4688
23) Fisher RM, Gertow K: Fatty acid transport proteins and insulin resistance. Curr Opin Lipidol, 2005; 16: 173-178
24) Labonté ED, Camarota LM, Rojas JC, Jandacek RJ, Gilham DE, Davies JP, Ioannou YA, Tso P, Hui DY, Howles PN: Reduced absorption of saturated fatty acids and resistance to diet induced obesity and diabetes by ezetimibe-treated and Npc1l1-/- mice. Am J Physiol Gastrointest Liver Physiol, 2008; 295: G776-G783
25) Yen CLE, Stone SJ, koliwad S, Harris C, Farese RV: DGAT enzymes and triacylglycerol biosynthesis. J Lipid Res, 2008; 49: 2283-2301
26) Sampath H, Miyazaki M, Dobrzyn A, Ntambi JM: Stearoyl-CoA desaturase-1 mediates the pro-lipogenic effects of dietary saturated fat. J Biol Chem, 2007; 282: 2483-2493
27) Man WC, Miyazaki M, Chu K, Ntambi J: Colocalization of SCD1 and DGAT2: implying preference for endogenous monounsaturated fatty acids in triglyceride synthesis. J Lipid Res, 2006; 47: 1928-1939
28) Hirano K, Young SG, Farese RV Jr, Ng J, Sande E, Warburton C, Powell-Braxton LM, Davidson NO: Targeted disruption of the mouse apobec-1 gene abolishes apolipoprotein B mRNA editing and eliminates apolipoprotein B48. J Biol Chem, 1996; 271: 9887-9990
29) Maris C, Masse J, Chester A, Navaratnam N, Allain FHT: NMR structure of the apoB mRNA stem-loop and its interaction with the C to U editing APOBEC1 complementary factor. RNA, 2005; 11: 173-186
30) Chester A, Weinreb V, Carter CW, Navaratnam N: Optimization of apolipoprotein B mRNA editing by APOBEC1 apoenzyme and the role of its auxiliary factor, ACF. RNA, 2004; 10: 1399-1411
31) Blanc V, Henderson JO, Newberry EP, Kennedy S, Luo J, Davidson NO: Targeted deletion of the murine apobec-1 complementation factor (acf) gene results in embryonic lethality. Mol Cell Biol, 2005; 25: 7260-7269

THE JOURNAL OF BIOLOGICAL CHEMISTRY VOL. 285, NO. 41, pp. 31337–31347, October 8, 2010

Isoform-specific Intermolecular Disulfide Bond Formation of Heterochromatin Protein 1 (HP1)*[S]

Received for publication, June 19, 2010, and in revised form, July 26, 2010 Published, JBC Papers in Press, August 1, 2010, DOI 10.1074/jbc.M110.155788

Shuichiro Higo[‡], Yoshihiro Asano[‡§¶], Hisakazu Kato[§], Satoru Yamazaki[¶], Atsushi Nakano[‡], Osamu Tsukamoto[¶], Osamu Seguchi[¶], Mitsutoshi Asai[‡], Masanori Asakura[¶], Hiroshi Asanuma[¶], Shoji Sanada[‡], Tetsuo Minamino[‡], Issei Komuro[‡], Masafumi Kitakaze[¶], and Seiji Takashima[‡§1]

From the Departments of [‡]Cardiovascular Medicine and [§]Molecular Cardiology, Osaka University Graduate School of Medicine, Suita, Osaka 565-0871 and the [¶]Department of Cardiovascular Medicine, National Cardiovascular Center, Suita, Osaka 565-8565, Japan

Three mammalian isoforms of heterochromatin protein 1 (HP1), α, β, and γ, play diverse roles in gene regulation. Despite their structural similarity, the diverse functions of these isoforms imply that they are additionally regulated by post-translational modifications. Here, we have identified intermolecular disulfide bond formation of HP1 cysteines in an isoform-specific manner. Cysteine 133 in HP1α and cysteine 177 in HP1γ were involved in intermolecular homodimerization. Although both HP1α and HP1γ contain reactive cysteine residues, only HP1γ readily and reversibly formed disulfide homodimers under oxidative conditions. Oxidatively dimerized HP1γ strongly and transiently interacted with TIF1β, a universal transcriptional co-repressor. Under oxidative conditions, HP1γ dimerized and held TIF1β in a chromatin component and inhibited its repression ability. Our results highlight a novel, isoform-specific role for HP1 as a sensor of the cellular redox state.

Heterochromatin protein 1 (HP1) was originally characterized as an abundant protein that binds pericentric heterochromatin (1). HP1 acts as a scaffold-like molecule, which is composed of two conserved domains as follows: the chromodomain (CD)[2] and the chromoshadow domain (CSD). The variable hinge region separates these two domains (2). The CD recognizes methylated lysine 9 of histone H3 (H3K9), which recruits HP1 to specific sites within the genome (3–5). The CSD promotes HP1 homodimer formation and provides a surface for interaction with a variety of other chromatin proteins (6, 7). Although genetic experiments previously revealed that HP1 works as a repressor of gene activation by propagation of a heterochromatin structure, emerging evidence has elucidated its diverse functions other than gene silencing (8). Some of these functions are regulated in an isoform-specific manner (9).

In vertebrates, three isoforms of HP1 exist as follows: α, β, and γ, all of which share highly conserved domains. Tethering any HP1 isoform upstream of a promoter equally triggers gene silencing concomitant with local chromatin condensation and an increase in H3K9 methylation (10–12), indicating their common silencing ability. However, nonredundant functions (13, 14), different binding affinities to other proteins (15–17) and different localizations in tissues (18, 19), of these three HP1 isoforms imply that α, β, and γ are functionally diverse. Furthermore, recent evidence clarified apparently opposite functions of HP1 isoforms, *e.g.* a role in transcriptional activation or in transcriptional elongation (20, 21). One mechanism that could account for such functional diversity of HP1 isoforms is post-translational modification, which could cause conformational changes in the molecule. In fact, reversible modifications of HP1 (*e.g.* phosphorylation) can modulate its function in response to various stimuli or cellular environments, suggesting an active role for HP1 beyond its known function as a marker of heterochromatin (17, 22). However, the precise modulatory mechanism across three HP1 isoforms that leads to functional differences remains to be elucidated.

Here, we identified isoform-specific disulfide bond formation as a novel post-translational modification of HP1. We analyzed the biochemical and functional characteristics of this oxidative modification. These data may offer a new insight into a novel role for HP1 during the cellular response to oxidative stress.

EXPERIMENTAL PROCEDURES

Materials—We used the following commercially available materials for Western blotting: anti-HP1α (H2164, Sigma; 19s2, Millipore); anti-HP1β (MAB3448, Chemicon); anti-HP1γ (42s2, Millipore); anti-FLAG M2-peroxidase antibody (Sigma); anti-histone H3 (ab1791, Abcam); anti-GAPDH (MAB374, Chemicon); and anti-TIF1β (4123, Cell Signaling). We also used anti-FLAG M2 affinity gel for immunoprecipitation. We used menadione (Sigma), H_2O_2 (Wako), and hydroxytamoxifen (4-OHT) (Sigma) for cell treatment.

Cell Fractionation—Cells were lysed with hypotonic lysis buffer (10 mM HEPES, pH 7.9, 1.5 mM $MgCl_2$, and 10 mM KCl) with 0.5% Nonidet P-40 and centrifuged at 20,000 × *g* for 5 min.

* This work was supported by grants-in-aid from the Ministry of Health, Labor, and Welfare of Japan, grants-in-aid from the Ministry of Education, Culture, Sports, Science, and Technology of Japan, grants from the Japan Heart Foundation, grants from the Japan Cardiovascular Research Foundation, a grant from the Japan Society for the Promotion of Science, Mochida Memorial Foundation for Medical and Pharmaceutical Research, Japan Medical Association, Japan Incurable Diseases Research Foundation, Osaka Medical Research Foundation for Incurable Diseases, Suzuken Memorial Foundation, and Japan China Medical Association.

[S] The on-line version of this article (available at http://www.jbc.org) contains supplemental Figs. S1–S4, "Experimental Procedures," and additional references.

[1] To whom correspondence should be addressed. Tel.: 81-6-6879-3472; Fax: 81-6-6879-3473; E-mail: takasima@medone.med.osaka-u.ac.jp.

[2] The abbreviations used are: CD, chromodomain; CSD, chromoshadow domain; HUVEC, human umbilical vein endothelial cell; 4-OHT, hydroxytamoxifen.

The supernatant was collected as the cytosolic fraction. Extraction buffer (20 mM HEPES, pH 7.9, 1.5 mM $MgCl_2$, 0.42 M NaCl, 0.2 mM EDTA, 25% glycerol) was added to the pellet, and ultrasonic agitation was performed (30-s sonication with 30-s interval, 4–6 times at 0 °C; Bioruptor, CosmoBio). The suspension was incubated for 15 min at 4 °C and centrifuged at 20,000 × *g* for 10 min. The supernatant was collected as the nuclear extract.

Column Chromatography—For anion exchange, whole cells were lysed with buffer A (20 mM Tris, pH 8.0, 5% acetonitrile) containing 5 mM EDTA and 1% Nonidet P-40 and incubated at 4 °C for 15 min. The lysate was centrifuged at 20,000 × *g* for 5 min, and the supernatant was filtered and loaded onto an anion-exchange column (Q-Sepharose High Performance, GE Healthcare) pre-equilibrated with buffer A. After unbound samples were washed, protein was eluted with a linear gradient (0–100%) of buffer B (buffer A with 1.0 M NaCl). For reverse-phase HPLC, purified protein samples and nuclear extracts were prepared with 0.3% trifluoroacetic acid (TFA) and 20% acetonitrile and applied to a phenyl reverse-phase column (4.6 × 250 mm; Nakalai Tesque). Bound proteins were eluted by a segmented linear gradient of increasing concentrations of buffer B (acetonitrile and 0.1% TFA) in buffer A (0.1% TFA) at a flow rate of 0.5 ml/min. Buffer B was increased at a rate of 1.0%/fraction (fast gradient) or 0.2%/fraction (slow gradient). Collected fractions were dried by a centrifugal evaporator and reconstituted with SDS sample buffer with or without 2.5% 2-mercaptoethanol (reducing or nonreducing conditions, respectively).

Triton Extraction—Triton extraction was carried out as described previously with modification (23). Cells were lysed with a hypotonic lysis buffer with 0.5% Nonidet P-40 and centrifuged at 20,000 × *g* for 5 min (as described above). The pellet was lysed in extraction buffer with 0.2% Triton X-100, incubated on ice for 30 min, and centrifuged at 20,000 × *g* for 5 min. The supernatant was kept as a Triton-soluble fraction. The remaining pellet was lysed in SDS sample buffer (250 mM Tris, 5% SDS, and 5% glycerol) with or without 2.5% 2-mercaptoethanol (reducing or nonreducing conditions, respectively), and ultrasonic agitation was performed as described above. After centrifugation at 20,000 × *g* for 5 min, the supernatant was kept as a Triton-insoluble fraction.

RNAi Knockdowns and Generation of HEK293T Stable Cells—Lentiviral particles derived from the pLKO.1-puro-containing shRNA sequence were purchased from the Mission shRNA library (Sigma). The oligonucleotide sequences of the shRNA were as follows: shRNA-6, CGACGTGTAGTGAATGGGAAA; and shRNA-7, GCGTTTCTTAACTCTCAGAAA. Lentiviral particles were used to transduce human umbilical vein endothelial cells (HUVECs) or HEK293T cells in the presence of 8 μg/ml Polybrene. To generate a HEK293T stable cell line, the infected cells were selected with 1 μg/ml puromycin. The stable cells in which HP1γ was almost completely depleted were next transfected with pEF-DEST51 HP1γ-FLAG WT or a C177S mutant (cloned from murine cDNA and resistant to shRNA), and the stable cells were selected with 5 μg/ml blasticidin.

GAL4-luciferase Reporter Assay—pC3-ERHBD-GAL4 or pC3-ERHBD-GAL4-KAP1 (TIF1β) with pGL4.31-PSV40-GAL4UAS were transfected using Lipofectamine 2000 into subconfluent HEK293T stable cells that were passaged 1 day before transfection. After 24 h, 0.04% ethanol or 4-OHT (500 nM) was added to the culture medium. Forty eight h after transfection, luciferase activity was measured by a luminometer (Lumat LB9507). Intranuclear mRNA levels of luciferase were measured as follows. Twenty four h after transfection, 4-OHT (500 nM) was added to the culture medium. Forty eight h after transfection, cells were lysed with a hypotonic lysis buffer with 0.5% Nonidet P-40 and centrifuged at 20,000 × *g* for 5 min (as described above). From the nuclear pellet, total RNA was isolated using RNA-Bee (Cosmo Bio). Total RNA was treated with DNase (Turbo DNA-free, Applied Biosystems) and was reverse-transcribed using a high capacity cDNA reverse transcription kit (Applied Biosystems). Luciferase mRNA levels were measured by real time quantitative PCR (SYBR Green ER, Invitrogen). Firefly luciferase cDNA was amplified using the following primers: 5′-TACCCACTCGAAGACGGGAC-3′ and 5′-ACTCGGCGTAGGTAATGTCCACCTC-3′. Human 18 S ribosomal RNA was measured using the following primers: 5′-GTAACCCGTTGAACCCCATT-3′ and 5′-CCATCCAATCGGTAGTAGCG-3′. The relative levels of luciferase mRNA were normalized to the mRNA levels of 18 S ribosomal RNA.

RESULTS

HP1α Forms Dimers via Disulfide Bonds through Cysteine 133—During purification of HP1α in our previous work (24), we found that endogenous HP1α separates into two peaks by fractionation using reverse-phase HPLC. To confirm this finding, we fractionated whole cell lysates from HEK293T cells using two-step column chromatography (Fig. 1*A*). Endogenous HP1α was eluted at a salt concentration ranging from 0.3 to 0.35 M on a Q-Sepharose anion-exchange column (Fig. 1*D*, *top panel*). We applied this single peak to a reverse-phase column. After elution with a fast gradient, HP1α was still detected as a single peak (Fig. 1*D*, *2nd panel*). However, when eluted with a slow gradient, HP1α separated into two peaks representing a hydrophilic and a hydrophobic form (Fig. 1*D*, *3rd panel*). Two other HP1α antibodies against different epitopes also detected both bands (data not shown), suggesting that these were biochemically different forms of HP1α. Even after direct fractionation of the nuclear extract, which includes the bulk of HP1α protein (Fig. 1*B*), endogenous HP1α showed a similar bimodal distribution (Fig. 1*D*, *4th panel*). In other primary cells (HUVECs, neonatal rat cardiomyocytes, and rat cardiac fibroblasts), similar bimodal peaks were observed (supplemental Fig. S1). In contrast, recombinant HP1α expressed in *Escherichia coli* (Fig. 1*C*) exhibited only one peak with elution characteristics similar to those of the hydrophilic peak under the same separating condition used for the endogenous protein (Fig. 1*D*, *bottom panel*). These data suggest that two different forms of HP1α endogenously exist in multiple cell types and that the late-eluted hydrophobic species may be a post-translationally modified form.

To further elucidate the molecular characteristics of these two forms of HP1α, we used recombinant FLAG-tagged HP1α (HP1α-FLAG). As with endogenous HP1α, HP1α-FLAG existed mainly as a nuclear protein (Fig. 1*E*) and exhibited the

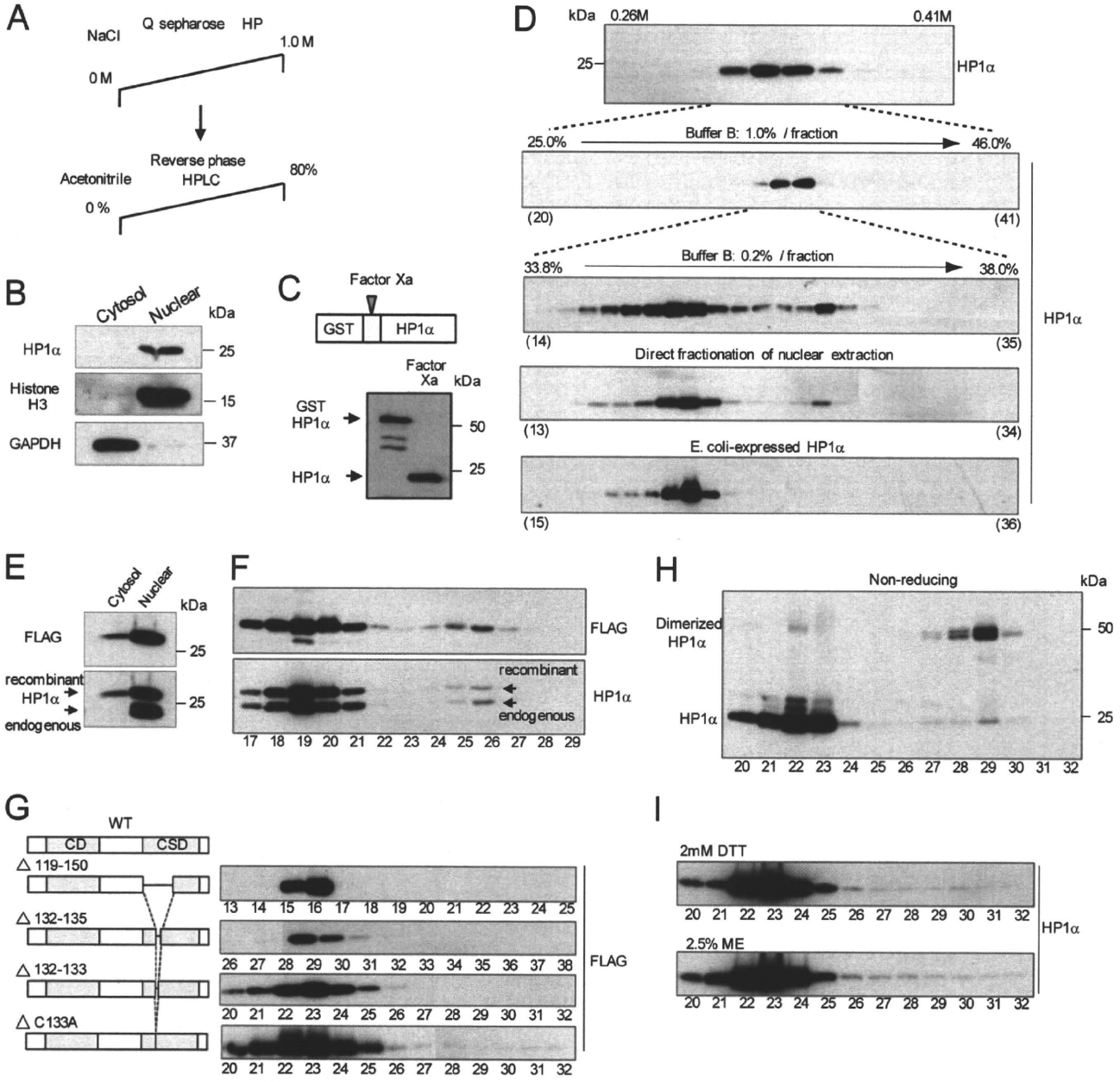

FIGURE 1. **Endogenous HP1α shows a bimodal distribution after protein purification by reverse-phase HPLC.** The late-eluted fraction of HP1α is oxidatively modified to form a disulfide bond. *A*, schematic representation of HP1α purification from cell lysates using sequential column chromatography. *B*, equal quantities of cytosolic and nuclear fractions from HEK293T cells were resolved by SDS-PAGE and probed with the indicated antibodies. *C*, GST-HP1α expressed in *E. coli* was purified and cleaved by Factor Xa (*upper panel*) and detected with anti-HP1α antibody (*lower panel*). *D*, HEK293T cell lysate was fractionated by a Q-Sepharose HP anion-exchange column. Eluted fractions were resolved by reducing SDS-PAGE and probed with anti-HP1α antibody (*top panel*). The *x* axis at the *upper edge* indicates salt concentration. HP1α fractions eluted from the anion-exchange column were next applied to a phenyl reverse-phase column. The fractions were eluted by a fast gradient (buffer B, 1.0% increase of acetonitrile concentration/fraction, *2nd panel from the top*) or by a slow gradient (buffer B, 0.2%/fraction, *3rd panel from the top*). Nuclear extraction from HEK293T cells (*4th panel from the top*) or HP1α purified from *E. coli* (*bottom panel*) was fractionated with the same slow gradient. The eluted fractions were resolved by reducing SDS-PAGE and probed with anti-HP1α antibody. *E*, equal quantities of cytosolic and nuclear fractions from HEK293T cells expressing HP1α-FLAG were resolved by SDS-PAGE and probed with the indicated antibodies. *F*, nuclear extract from HEK293T cells expressing HP1α-FLAG was directly applied to a reverse-phase column, and the eluted fractions were resolved by reducing SDS-PAGE and probed with the indicated antibodies. *G*, diagrams of the representative deletion mutant or point mutant of the HP1α protein during stepwise mutation analysis (*left column*). Nuclear extractions from HEK293T cells expressing each mutant protein were fractionated by reverse-phase HPLC, resolved by SDS-PAGE, and probed with anti-FLAG antibody (*right column*). *H*, endogenous HP1α was purified from the HEK293T cell lysate as shown in *A*. The fractions eluted from the reverse-phase column were resolved by SDS-PAGE under nonreducing conditions and probed with anti-HP1α antibody. *I*, nuclear extract from HEK293T cells was incubated with 2 mM DTT or 2.5% 2-mercaptoethanol (*ME*) for 30 min at 4 °C and then applied to a reverse-phase column. The eluted fractions were resolved by SDS-PAGE and probed with anti-HP1α antibody. *D* and *F–I*, the *x* axis at the *lower edge* indicates fraction numbers.

same bimodal distribution after reverse-phase HPLC (Fig. 1*F*). Thus, we concluded that HP1α-FLAG undergoes the same modification as endogenous HP1α, validating the use of the tagged protein for further analysis. Initially, we attempted to detect the specific modification directly by matrix-assisted laser desorption/ionization and time-of-flight mass spectrometry (MALDI-TOF/MS) (supplemental Fig. S2, *A–C*). Although we detected peptide masses from both fractions corresponding to ~75% of the entire HP1α sequence (supplemental Fig. S2*B*), we did not detect any distinct features in the mass spectra under two different digestion conditions (trypsin or Asp-N) (supplemental Fig. S2*C*). We next tried to detect a modified residue by making multiple, stepwise mutations throughout the entire HP1α molecule. We hypothesized that HP1α-FLAG lacking the modified residue would fractionate into a single peak by reverse-phase HPLC. First, we thoroughly screened the CD and hinge region, both of which are reported to be post-translationally modified (17, 22). However, we could not determine any specific amino acid residue from the mutational analysis (supplemental Fig. S2*D*). Second, we screened the CSD (supplemental Fig. S2*E*) and found that a deletion mutant lacking residues 119–150 (Δ119–150) was eluted as a single peak. We further narrowed down the deleted sequence 119–150 and finally found that a mutant in which cysteine 133 (Cys-133) was replaced by alanine (C133A) was eluted as a single peak (Fig. 1*G*). These data suggest that the single cysteine 133 residue is responsible for the separation of the hydrophobic fraction of HP1α.

Among post-translational modifications of cysteine, oxidation is a common feature. The thiol side chain can be oxidized to sulfenic acid (-SOH), sulfenyl amide (–SN), a disulfide bond (–SS–) or an irreversibly oxidized form (25). We examined the electrophoresis pattern of the two separated fractions of HP1α under nonreducing conditions and found that the hydrophobic form of HP1α shifted to a molecular weight twice its size, indicating that this HP1α formed a homodimer (Fig. 1*H*). In contrast, the mobility of the hydrophilic HP1α was unchanged. Because this dimer was nondissociable both under the strong acidic conditions of the reverse-phase HPLC and under the denaturing conditions during SDS-PAGE, it seemed to be linked by a covalent bond. Pretreatment with reducing agents, such as 2 mM DTT or 2.5% 2-mercaptoethanol, completely abolished the hydrophobic fraction (Fig. 1*I*). Taken together, these data suggest that endogenous HP1α dimerizes by intermolecular disulfide bond formation via Cys-133.

HP1α and HP1γ Both Possess an Isoform-specific Cysteine Residue for Disulfide Bond Formation—The sequence identity among the three HP1 isoforms is remarkably high (Fig. 2*A*), with up to 80% homology in the CSD. However, Cys-133 is specific to HP1α and is replaced by a serine in HP1β and HP1γ (highlighted in *red* in Fig. 2*A*). Therefore, we evaluated whether this oxidative modification was specific for HP1α. Endogenous HP1β was fractionated as a single peak by reverse-phase HPLC. However, endogenous HP1γ was isolated as two separate peaks (Fig. 2*B*). Both the hydrophilic and the hydrophobic fractions of HP1γ were eluted independently of those of HP1α suggesting that these two isoforms did not interact with each other during reverse-phase HPLC fractionation. Similar to HP1α, the hydrophobic form of HP1γ also dimerized (Fig. 2*C*). HP1β contains only two cysteines, both of which are conserved among the isoforms (Cys-59 and Cys-160 of HP1α; highlighted in *blue* in Fig. 2*A*). HP1γ has three cysteines, and one of the cysteines, Cys-177, is an isoform-specific residue located in the C terminus of the CSD. This residue is replaced by tyrosine in HP1α and HP1β (highlighted in *red* in Fig. 2*A*). Mutational analysis of these cysteine residues revealed that only isoform-specific Cys-133 of HP1α and Cys-177 of HP1γ were involved in dimerization (Fig. 2*D*). Mutating the corresponding residues of HP1β, Ser-129 (matched to Cys-133 of HP1α) or Tyr-173 (matched to Cys-177 of HP1γ), to cysteines created the late-eluted hydrophobic form (Fig. 2*E*). These hydrophobic forms of HP1β dimerized similarly with HP1α and HP1γ (Fig. 2*F*). The other two HP1β mutants, S141C and S162C, did not form disulfide bonds. Together, these data suggest that even though their overall structures are highly conserved, endogenous HP1α and HP1γ possess isoform-specific cysteine residues involved in the intermolecular disulfide bond formation. These two positions of the disulfide-linked cysteines are structurally sensitive to oxidation within the CSD.

HP1γ Is More Sensitive to Oxidation than HP1α in Vitro—We tested whether the differences in the positions of the modified cysteine residues between HP1α and HP1γ influenced their sensitivity to oxidation *in vitro*. Under mild oxidative conditions, only a low level of dimerized HP1α was detected even after a long exposure to air oxidation (Fig. 3*A*, *left panels*). In contrast, under the same conditions, HP1γ was easily oxidized to form disulfide bonds (Fig. 3*A*, *right panels*). Treatment with DTT reversed the disulfide formation of HP1γ. These data indicate that HP1γ is more sensitive to oxidation and more readily forms a disulfide dimer *in vitro*.

Using purified and oxidized HP1γ-FLAG, the intermolecular disulfide bond was confirmed by MALDI-TOF/MS analysis. The late-eluted dimerized fraction of HP1γ-FLAG was resolved by nonreducing SDS-PAGE, and the excised band was divided into two samples. One sample was reduced, carbamidomethylated with iodoacetamide, and digested by trypsin. The other sample was directly digested without pretreatment. The expected digested peptide, including Cys-177, consisted of the C terminus of HP1γ and lysine residue within the linker peptide (Fig. 3*B*). The mass spectrum peak of 3084.32, which was detected only in the nonreduced sample, corresponded to the estimated mass of the dimeric peptide connected by a disulfide bond via Cys-177 (3084.35) (Fig. 3*C*, *upper panel*). In contrast, the peak at 1600.68, which was detected only in the reduced sample, corresponded to the estimated mass of the monomeric peptide, including carbamidomethylated Cys-177 (1600.71) (Fig. 3*C*, *lower panel*). No other significant mass spectral peaks from the intermolecular disulfide bond were detected.

HP1γ, but Not HP1α, Readily Forms Disulfide Bonds under in Vivo Oxidative Conditions—We assessed whether this oxidative modification was promoted under *in vivo* oxidative conditions using a pro-oxidant agent, 2-methyl-1,4-naphthoquinone (menadione), which caused oxidative stress in cells (Fig. 4*A*) (26). Menadione treatment caused a dose- and time-dependent increase in the disulfide bond formation of HP1γ in COS7 cells (Fig. 4*B*, *left two panels*). The disulfide dimerization of HP1γ

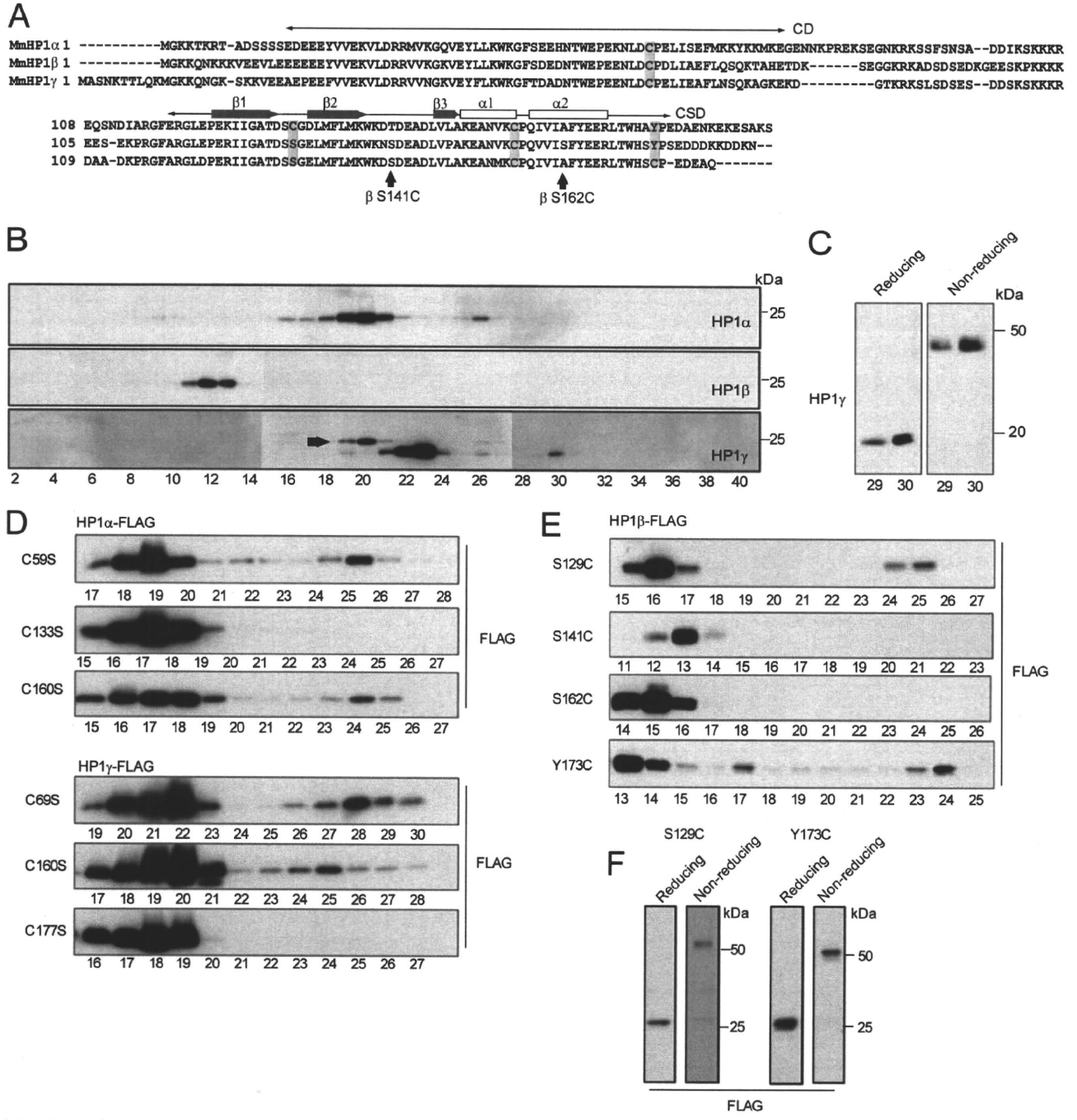

FIGURE 2. **Both HP1α and HP1γ possess isoform-specific cysteine residues that are oxidatively modified to form disulfide bonds.** *A*, amino acid sequence alignment among mouse HP1 isoforms. *Crosswise two-headed arrows* indicate the N-terminal CD and C-terminal CSD. The *bold blue arrow* and *bold white line* along the CSD indicate β-sheet and α-helix, respectively. *Blue highlights* represent the following: two cysteine residues conserved among the HP1 family (Cys-59 and Cys-160; HP1α). *Red highlights* represent the following: position of the cysteine residue specific to HP1α (Cys-133) or HP1γ (Cys-177). The *arrowhead* indicates the position of the mutated HP1β serine residue (shown in *E*). *B*, nuclear extract from HEK293T cells was directly applied to a reverse-phase column, and the eluted fractions were resolved by SDS-PAGE and probed with anti-HP1α, -β, or -γ antibodies. The immunoblotting procedure was performed by consecutive stripping and reprobing with each antibody of the same membrane. The *upper band* of fraction 20 in the *bottom panel* (*arrowhead*) indicates the residual signal from hydrophilic HP1α. *C*, hydrophobic fractions of HP1γ purified from HEK293T cells (as shown in Fig. 1*A*) were resolved by SDS-PAGE under reducing or nonreducing conditions and probed with anti-HP1γ antibody. *D*, nuclear extract from HEK293T cells expressing each HP1α-FLAG (*top three panels*) or HP1γ-FLAG (*bottom three panels*) with a cysteine-to-serine mutation was fractionated by reverse-phase HPLC, resolved by SDS-PAGE, and probed with anti-FLAG antibody. *E*, nuclear extract from HEK293T cells expressing HP1β-FLAG with each serine-to-cysteine or tyrosine-to-cysteine mutation was fractionated by reverse-phase HPLC, resolved by SDS-PAGE, and probed with anti-FLAG antibody. *F*, late-eluted hydrophobic fraction of the HP1β-FLAG mutant (S129C or Y173C) was resolved by reducing or nonreducing SDS-PAGE and probed with anti-FLAG antibody. *B–E*, the *x* axis at the lower edge indicates fraction numbers.

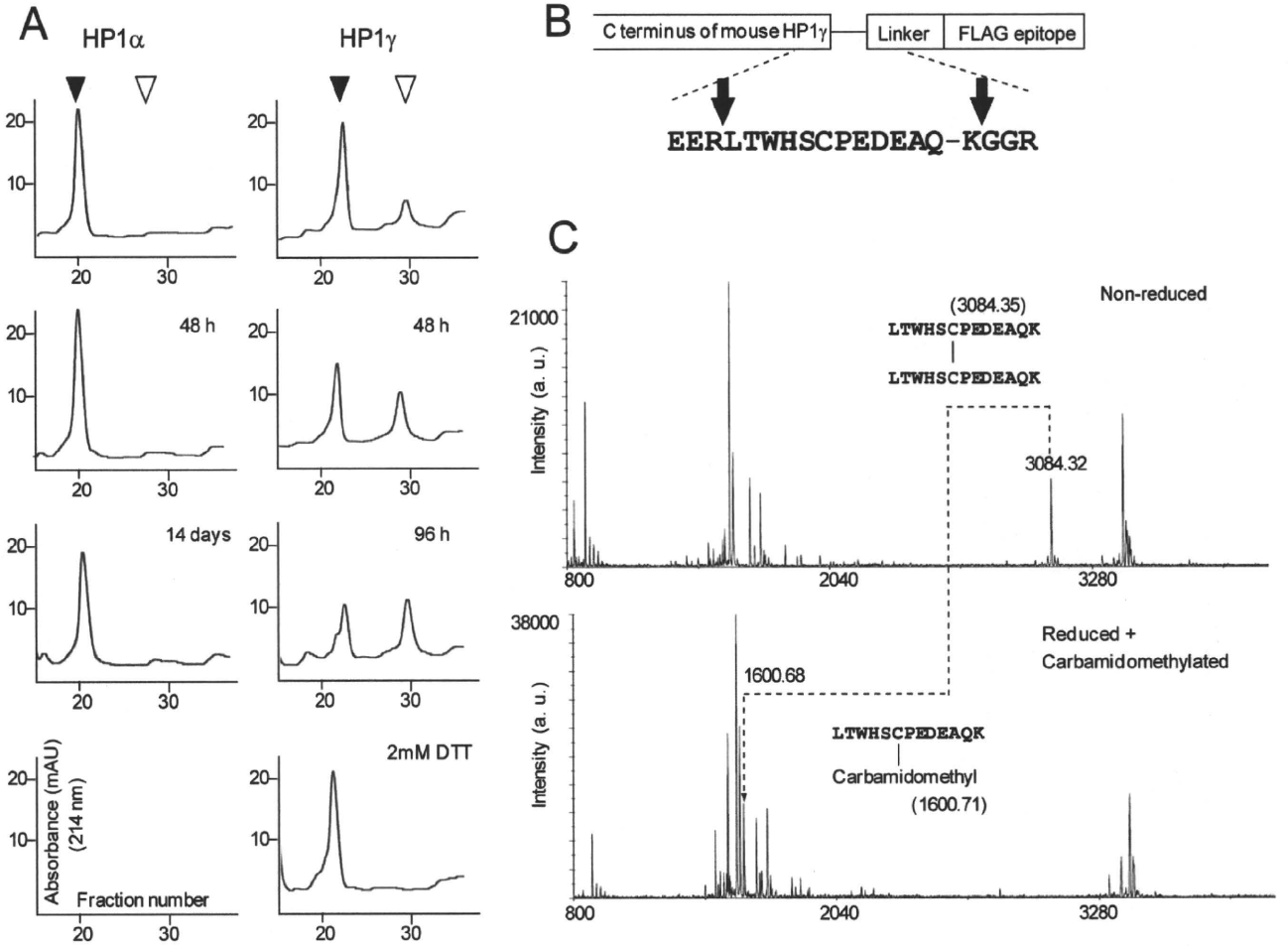

FIGURE 3. **HP1γ is more sensitive to oxidation than HP1α *in vitro*.** MALDI-TOF/MS analysis confirms the disulfide bond formation of HP1γ via Cys-177. *A*, HP1α-FLAG or HP1γ-FLAG expressed in COS7 cells was purified by an anion-exchange column and further fractionated by reverse-phase HPLC. The HPLC absorption pattern profiles at 214 nm are shown. *Black* or *white arrowheads* indicate the fraction of hydrophilic (monomer) or hydrophobic (dimer) forms of HP1, respectively. HP1α-FLAG was fractionated by reverse-phase HPLC immediately after anion exchange (*left top*) or after air oxidation at 4 °C for 48 h or 14 days. HP1γ-FLAG was fractionated immediately after anion exchange (*right top*) or after air oxidation at 4 °C for 48 or 96 h. The HP1γ-FLAG oxidized for 6 days was incubated with 2 mM DTT at 4 °C for 1 h and fractionated by reverse-phase HPLC (*right bottom*). *B*, C-terminal structure of HP1γ-FLAG. *Arrowheads* indicate the trypsin digestion positions. *C*, mass spectra from MALDI-TOF/MS analysis of nonreduced (*upper panel*) or reduced, carbamidomethylated (*lower panel*) HP1γ-FLAG. The expected sequence and estimated mass (*m/z*) of the digested peptide are shown.

was rapidly formed within minutes and was only formed via Cys-177 (Fig. 4*C*). The I165E mutation, which inhibits both noncovalent α-helix dimer formation and proper nuclear localization (6–7), decreased, but not completely, the amount of disulfide dimers of HP1γ (supplemental Fig. S3*A*). These data suggest that the oxidative dimerization of HP1γ requires the proper localization and formation of constitutive, noncovalent dimers.

In contrast to HP1γ, an increase in dimerized HP1α was not observed under the same *in vivo* oxidative conditions (Fig. 4*B*, *right panel*). The dimerized forms of HP1α and HP1γ under basal conditions were almost undetectable without using the large scale purification shown in Fig. 1 because of their relatively low abundance before oxidant treatment. Menadione treatment promoted HP1γ dimerization in various cells, but the extent of dimerization varied among cell types (supplemental Fig. S3*B*), suggesting that the reactivity of HP1γ to reactive oxygen species stimulation varied according to cell type. In each cell, an increase in dimerized HP1α was not observed (data not shown). These results demonstrate that there is a clear difference in oxidation sensitivity among HP1 family members. Although both HP1α and HP1γ have oxidation-sensitive cysteines in their sequences, HP1γ perceives oxidative conditions and is able to more readily form a disulfide dimer than HP1α.

In HEK293T cells, the dimerized HP1γ was subsequently reduced to the monomer form after removal of the oxidant (Fig. 4*D*, *upper panel*), but HP1γ remained dimerized when continuously exposed to the oxidants (Fig. 4*D*, *lower panel*), suggesting that this oxidative modification was reversible.

H_2O_2, known as an endogenous source of reactive oxygen species, also promoted dimerization of HP1γ (Fig. 4*E*). This effect of H_2O_2 was relatively weak in HEK293T cells when compared with the treatment of menadione. However, the same concentration of H_2O_2 substantially increased the amount of dimerized HP1γ in HUVECs (Fig. 4*E*, *lower panel*). Therefore, we further examined the molecular characteristics of the disulfide dimerization of HP1γ using HUVECs.

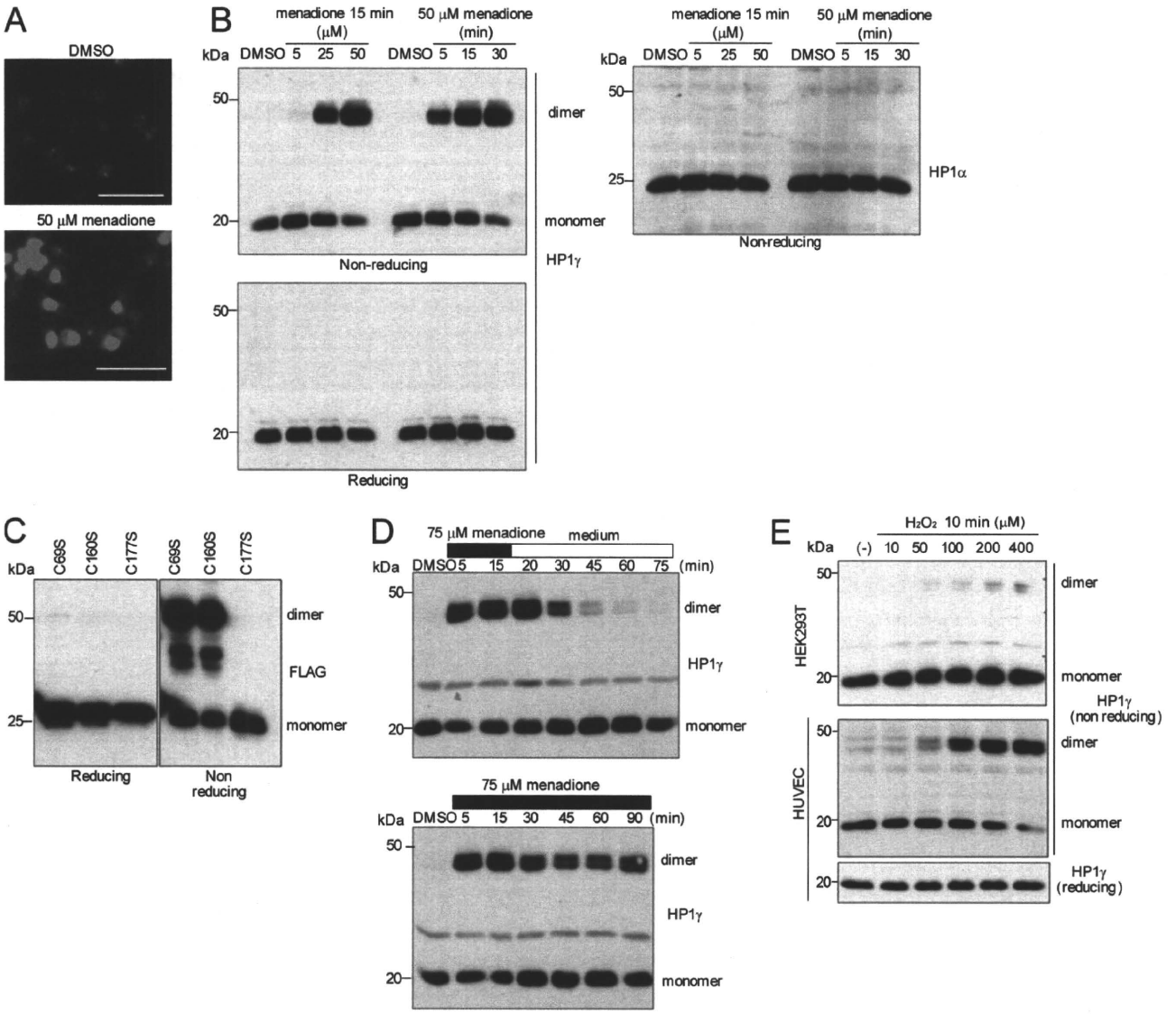

FIGURE 4. **HP1γ, but not HP1α, readily forms disulfide bonds under oxidative conditions.** *A*, after treatment with DMSO or 50 μM menadione for 15 min, COS7 cells were stained with 20 μM dihydroethidium for 30 min and monitored by fluorescence microscopy. *Bar*, 100 μm. *B*, COS7 cells treated with DMSO or menadione under the indicated conditions were lysed, resolved by nonreducing (*upper panel*) or reducing (*lower panel*) SDS-PAGE, and probed with anti-HP1γ antibody. The same membrane was reprobed with anti-HP1α antibody (*right panel*). *C*, COS7 cells expressing each cysteine-to-serine mutant HP1γ-FLAG were treated with 50 μM menadione for 15 min. Lysates were resolved by reducing (*left panel*) or nonreducing (*right panel*) SDS-PAGE and probed with anti-FLAG antibody. *D*, HEK293T cells were treated with 75 μM menadione for 15 min. Subsequently, the culture medium was exchanged for fresh medium (*upper panel*) or kept unchanged (*lower panel*). After incubation for the indicated time, cell lysates were resolved by nonreducing SDS-PAGE and probed with anti-HP1γ antibody. *E*, HEK293T cells and HUVECs were treated with H_2O_2 under the indicated conditions. Cell lysates were resolved by SDS-PAGE and probed with anti-HP1γ antibody. *B–E*, cells were lysed with a buffer (10 mM Tris-HCl, pH 7.2, 150 mM NaCl, 1 mM EDTA, and 1% Nonidet P-40) containing 100 mM maleimide, a thiol-alkylating agent, to prevent artifactual oxidation.

Under Oxidative Conditions, HP1γ Strongly and Transiently Interacts with TIF1β and Holds It in a Chromatin Component—The CSD of HP1, which includes Cys-177 at its C terminus, creates a binding surface for other proteins (27). Therefore, disulfide modification of HP1γ may affect the interactions between HP1 and HP1-binding proteins. Because many candidate effectors that bind to HP1 exist (8), we screened the interacting proteins of HP1γ under oxidative conditions using metabolically radiolabeled HUVECs expressing recombinant HP1γ-FLAG transduced with adenovirus. Among the co-immunoprecipitated proteins, one protein band was detected after treatment with H_2O_2 (Fig. 5*A*, *arrowhead*). The bound protein was purified and analyzed by MALDI-TOF/MS. The amino acid sequence of the digested peptides corresponded to TIF1β (also known as TRIM28 or KAP1), which is a universal co-repressor of gene transcription and is a well known interacting partner of HP1 (28–31). Co-immunoprecipitation analysis showed that endogenous HP1γ strongly interacted with TIF1β in a dose-dependent manner after H_2O_2 treatment (Fig. 5*B*). TIF1β did not interact with HP1γ with a C177S mutation under oxidative conditions, suggesting that the disulfide bond formation of HP1γ enhanced the interaction of these proteins (Fig. 5*C*). When the oxidant was removed, TIF1β dissociated again from HP1γ, suggesting that this enhanced endogenous interac-

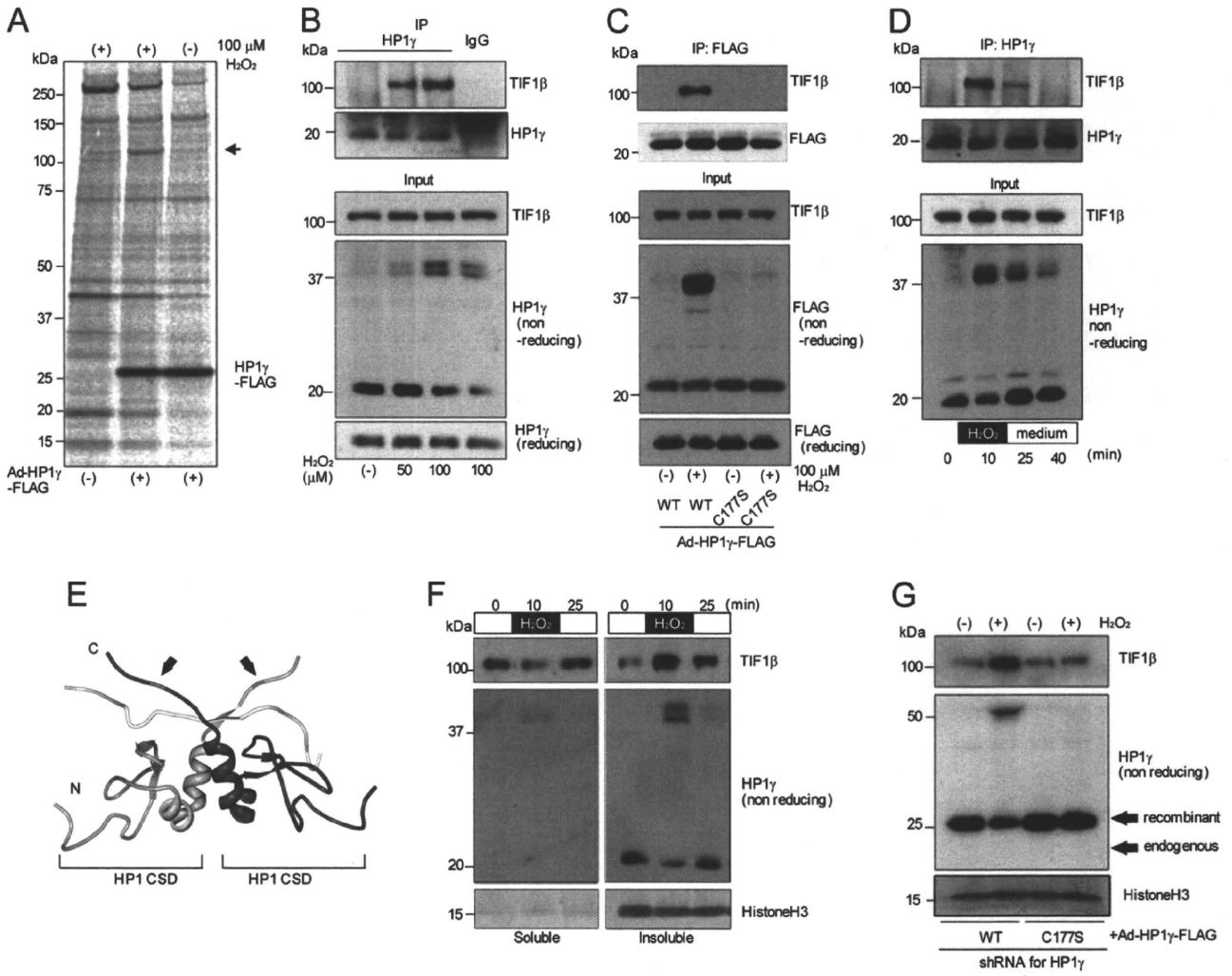

FIGURE 5. **HP1γ strongly interacts with TIF1β and promotes translocation of TIF1β to a chromatin component when dimerized under oxidative conditions.** *A*, HUVECs expressing HP1γ-FLAG (transduced by adenovirus) were metabolically labeled with [^{35}S]cysteine and -methionine for 6 h. Nontransduced cells were also labeled as a negative control. Forty eight h after transduction, the cells were treated with 100 μM H_2O_2 or control (water) for 10 min, lysed, and immunoprecipitated with anti-FLAG M2 affinity gel. Bound samples were resolved by reducing SDS-PAGE and visualized by autoradiography. The *arrow* indicates the protein band co-immunoprecipitated with HP1γ-FLAG only under the oxidative conditions. *B*, lysates from HUVECs treated with control (water) or H_2O_2 for 10 min were immunoprecipitated (*IP*) with anti-HP1γ antibody. Bound samples were resolved by SDS-PAGE and probed with the indicated antibodies. *C*, HUVECs expressing WT or C177S HP1γ-FLAG (transduced by adenovirus) were treated with 100 μM H_2O_2 for 10 min. Lysates were immunoprecipitated with anti-FLAG M2 affinity gel, and bound samples were resolved by SDS-PAGE and probed with the indicated antibodies. *D*, HUVECs were transiently treated with 100 μM H_2O_2. Lysates were immunoprecipitated with anti-HP1γ antibody, and bound samples were resolved by SDS-PAGE and probed with the indicated antibodies. *E*, structure of HP1 CSD noncovalent homodimer (*blue* and *cyan*) and P*XVXL* motif (*yellow*) complex (Protein Data Bank code 1s4z, modified using the WEB tool (43)). The position of Cys-177 in HP1γ is highlighted in *red* (*black arrows*). *F*, HUVECs were transiently treated with 100 μM H_2O_2. Soluble and insoluble nuclear fractions were obtained using Triton extraction. Each sample was resolved by SDS-PAGE and probed with the indicated antibodies. *G*, HUVECs were transduced with lentivirus expressing shRNA against HP1γ and adenovirus expressing shRNA-resistant HP1γ-FLAG WT or C177S mutant. Triton-insoluble fractions from these cells after H_2O_2 treatment were resolved by SDS-PAGE and probed with the indicated antibodies.

tion was transient (Fig. 5*D*). Structurally, disulfide dimerization via Cys-177 is formed at the C terminus of the CSD, just adjacent to the binding interface for the P*XVXL* motif, which is a well characterized binding sequence in HP1-interacting proteins, including TIF1β (Fig. 5*E*) (7).

We next examined the localization changes of these proteins before and after oxidant treatment. No remarkable change in localization was detected by immunostaining (data not shown). However, biochemical analysis using Triton extraction verified the TIF1β translocation. HP1γ existed mainly in the Triton-insoluble chromatin component, whereas TIF1β was distributed both in the soluble and the insoluble components (Fig. 5*F*). Under oxidative conditions, HP1γ dimerized and was maintained in the insoluble components. Concomitant with HP1γ dimerization, the insoluble component of TIF1β transiently increased. The knockdown of endogenous HP1γ combined with the replacement by a C177S mutant of HP1γ inhibited the translocation of TIF1β, suggesting that HP1γ held TIF1β on chromatin only when oxidized via Cys-177 (Fig. 5*G*). These data suggest that the intracellular redox state is transduced to the conformational and localization change of the repressor complex via oxidative modification of HP1γ.

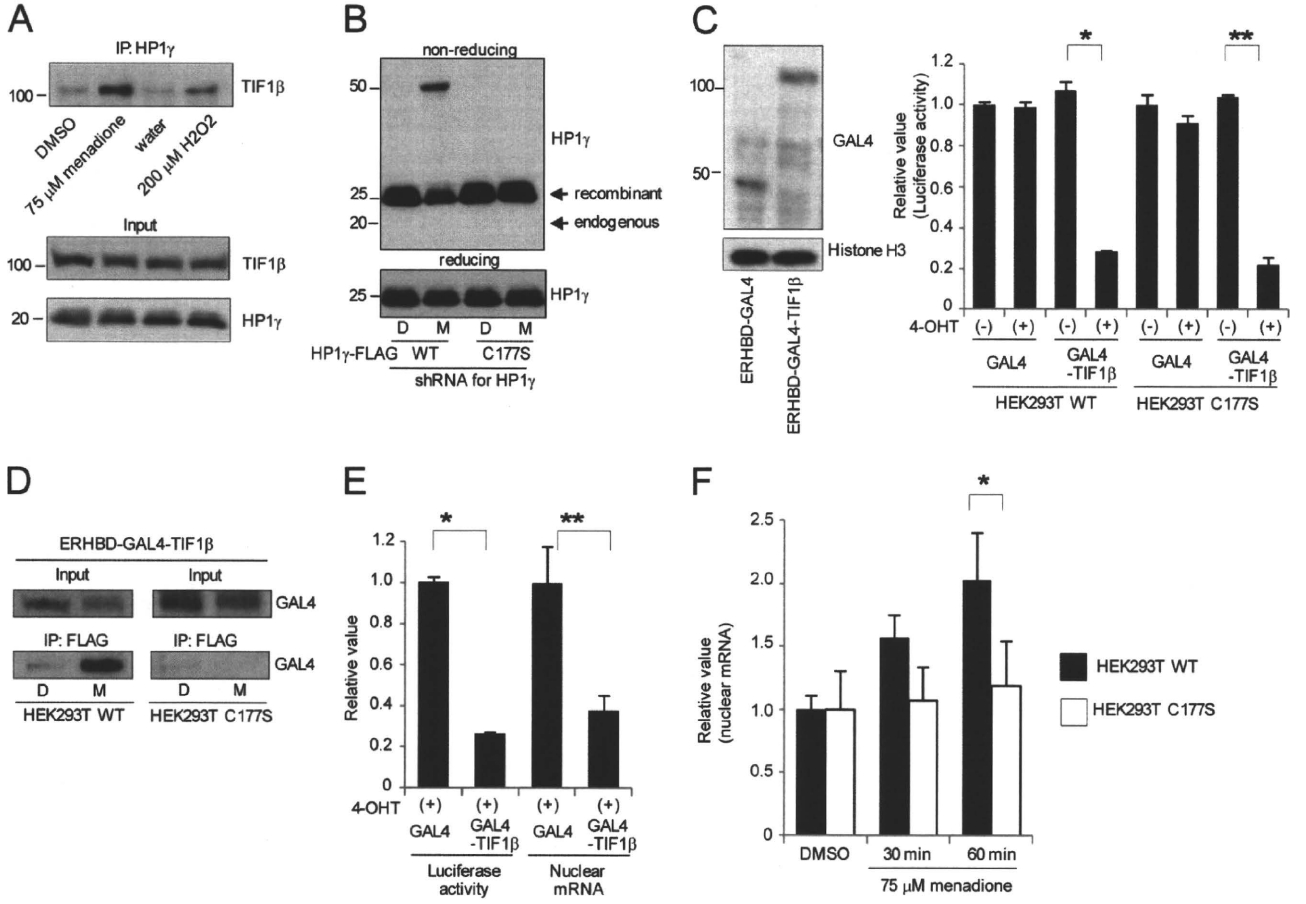

FIGURE 6. **Dimerized HP1γ under oxidative conditions inhibits the repression ability of TIF1β.** *A*, lysates from HEK293T cells treated with DMSO, 75 μM menadione, water, or 200 μM H_2O_2 for 15 min were immunoprecipitated (*IP*) with anti-HP1γ antibody. Bound samples were resolved by SDS-PAGE and probed with the indicated antibodies. *B*, HEK293T cells stably expressing shRNA for HP1γ and shRNA-resistant recombinant FLAG-tagged HP1γ were treated with DMSO or 75 μM menadione for 15 min. Cell lysates were resolved by nonreducing or reducing SDS-PAGE and probed with anti-HP1γ antibody. *D* indicates DMSO, and *M* indicates 75 μM menadione. *C*, lysates from HEK293T stable cells transfected with an ERHBD-GAL4 or ERHBD-GAL4-TIF1β fusion protein were resolved by SDS-PAGE and probed with the indicated antibodies (*left panel*). HEK293T stable cells were transfected with the plasmids encoding ERHBD-GAL4 or ERHBD-GAL4-TIF1β with the reporter plasmids. Twenty four h after transfection, 4-OHT was added to culture medium (500 nM). Forty eight h after transfection, luciferase activity was measured (*right panel*). The relative value was corrected by the value of the cells transfected with ERHBD-GAL4 without 4-OHT induction. Student's *t* test; *, **, $p < 0.01$. *D*, HEK293T stable cells expressing ERHBD-GAL4-TIF1β were treated with DMSO or 75 μM menadione for 15 min. Lysates were immunoprecipitated with anti-FLAG affinity gel. Bound samples were immunoblotted with anti-GAL4 antibody. *D* indicates DMSO, and *M* indicates 75 μM menadione. *E*, under the same conditions as *C*, luciferase transcription levels were determined both by protein enzymatic activity and intranuclear mRNA levels measured by quantitative PCR. Student's *t* test; *, **, $p < 0.01$. *F*, HEK293T stable cells expressing ERHBD-GAL4-TIF1β with 500 nM 4-OHT induction were treated with DMSO for 60 min or 75 μM menadione for the indicated time. Intranuclear luciferase mRNA levels at each time point were measured by quantitative PCR. The relative value was corrected by the value of the cells treated with DMSO. Two-way repeated measure analysis of variance; *, $p < 0.05$. The means ± S.D. as indicated by the *error bars* were determined from three independent experiments.

Dimerized HP1γ under Oxidative Conditions Inhibits the Repression Ability of TIF1β—To clarify whether the repression ability of TIF1β was promoted or inhibited when trapped by HP1γ under oxidative conditions, we used a GAL4-based transcriptional reporter assay. In HEK293T cells, menadione treatment promoted the disulfide dimerization of HP1γ and the interaction between HP1γ and TIF1β more prominently than H_2O_2 treatment (supplemental Fig. S3*B* and Figs. 4*E* and 6*A*). Therefore, we used menadione treatment for further analysis in HEK293T cells. We generated HEK293T cells stably expressing shRNA for HP1γ and shRNA-resistant recombinant FLAG-tagged HP1γ WT or C177S mutant. In these cells, endogenous HP1γ was almost completely depleted and was replaced by the dimerizable or undimerizable recombinant proteins (Fig. 6*B*). To evaluate the transcriptional repression ability of TIF1β, we transfected the plasmids encoding ERHBD-GAL4 as a control or ERHBD-GAL4-TIF1β fusion protein with the reporter plasmids in these cells (12, 32). The transcriptional regulatory activity of the ERHBD fusion protein is post-translationally controlled by the addition of 4-OHT to the culture medium (12). In our experimental conditions where ERHBD-GAL4 and ERHBD-GAL4-TIF1β were equally expressed (Fig. 6*C*, *left panel*), only ERHBD-GAL4-TIF1β repressed transcription of luciferase with 4-OHT (500 nM) in the HEK293T stable cells (Fig. 6*C*, *right panel*). The extent of repression was similar between the cells expressing either the HP1γ-FLAG WT or the C177S mutant under nonoxidative conditions. When the cells were treated with menadione, HP1γ-FLAG WT strongly interacted with ERHBD-GAL4-TIF1β as was similarly observed with endogenous proteins (Fig. 6*D*). To examine the transcrip-

tional change of the luciferase gene under oxidative conditions, we measured the intranuclear mRNA levels of luciferase by quantitative PCR instead of luciferase protein enzymatic activity (Fig. 6*E*). We chose this end point because the oxidation of HP1γ was too rapid to properly evaluate its effect on luciferase transcription by measuring luciferase protein enzymatic activity. Under these conditions, menadione treatment relieved the levels of luciferase transcription repressed by ERHBD-GAL4-TIF1β in the cells expressing HP1γ-FLAG WT but did not relieve the levels in the cells expressing the C177S mutant (Fig. 6*F*). These data suggest that dimerized HP1γ under oxidative conditions inhibits the repression ability of TIF1β.

It remained unclear whether the intranuclear redox-sensing mechanism through the oxidative modification of HP1γ plays a role in the cellular response to extrinsic oxidative stress. Therefore, we assessed the effect of this modification on cell survival under oxidative conditions using HEK293T cells stably expressing shRNA against HP1γ (supplemental Fig. S4*A*). Depletion of HP1γ using shRNA uniformly decreased cell viability under oxidative conditions induced by menadione treatment (supplemental Fig. S4*B*). For a rescue experiment, these stable clones were transduced with an adenoviral vector encoding WT HP1γ-FLAG or C177S HP1γ-FLAG. Both HP1γ vectors were cloned from murine cDNA and were resistant to shRNA against human HP1γ. Transduction of both adenoviral constructs at a multiplicity of infection of 20 resulted in nearly equal expression of recombinant HP1γ with endogenous HP1γ and yielded a similar disulfide dimerization pattern (supplemental Fig. S4*C*). Under these conditions, WT HP1γ-FLAG rescued cell viability after menadione treatment in each stable clone, but the C177S HP1γ-FLAG mutant did not rescue cell viability (supplemental Fig. S4*D*). These results suggest that HP1γ disulfide dimerization plays a pivotal role in cell survival under oxidative conditions.

DISCUSSION

In this study, we identified isoform-specific disulfide bond formation, which is a novel post-translational modification of HP1, using a unique column chromatography method. Biochemical analysis revealed two isoform-specific reactive cysteine residues, cysteine 133 in HP1α and cysteine 177 in HP1γ. In particular, HP1γ readily and reversibly formed disulfide dimers under oxidative conditions. Dimerized HP1γ strongly interacted with TIF1β and held it in a chromatin component. The GAL4 tethering repression assay revealed that the tight interaction of the repressor proteins had a reversing effect for transcriptional repression.

Several post-translational modifications of HP1 have been reported. Specifically, the linker region between the CSD and CD is highly amenable to post-translational modifications, especially phosphorylation that affects silencing activity or nuclear location of HP1 (17, 33–35). Also in the CD, Thr-51 of HP1β has been shown to be phosphorylated in response to DNA damage (22). More recently, a comprehensive proteomic analysis revealed that all HP1 isoforms are highly modified by phosphorylation, acetylation, methylation, and formylation both in the CD and in the CSD (36). Prior to this study, however, no oxidative modification of HP1 had been identified. Because oxidative modifications at cysteine residues would be easily disrupted under reducing conditions, such modifications may be detected only by the unique HPLC-based method used in this study and not by ordinary mass spectrometry analysis.

Both isoform-specific cysteines involved in forming disulfide bonds reside in a structurally flexible region of the CSD. Cys-133 of HP1α lies in the long loop between the β1 and β2 sheets, and Cys-177 of HP1γ lies in the C-terminal region. Introducing cysteine residues into these flexible sites of HP1β conferred the ability to form disulfide bonds, suggesting that these sites have specific structures in the oxidative center. Although both cysteines were reactive, a distinct difference of sensitivity to oxidation existed. Each location of reactive cysteines and the surrounding structure might determine the sensitivity of HP1α and -γ to oxidation. Under both *in vitro* and *in vivo* oxidative conditions, HP1γ readily formed disulfide bonds. In contrast, only minimal disulfide formation of HP1α by oxidation was observed under our experimental conditions. The reactivity of HP1α under oxidation might be observed under different conditions. Nonetheless, the isoform specificity and functional importance of Cys-133 in HP1α has been reported previously (15).

HP1 has been reported to form dimers via the CSD, but these dimers are not mediated by disulfide bonds or other covalent bonds (6, 37, 38). Thus, HP1 dimerizes in at least two ways. The interface of the noncovalently linked dimer involves a symmetrical interaction on helix α2 of the CSD (27) and creates a nonpolar groove structure, which is a binding site for the PXVXL motif in HP1-interacting proteins, such as TIF1β (Fig. 5*E*) (7). Because reactive cysteine 177 in HP1γ is located in the C terminus adjacent to the groove structure, disulfide bond formation at this site likely affects the binding affinity of HP1γ. Indeed, HP1γ strongly and transiently interacted with TIF1β and promoted its translocation to a chromatin component stringently depending on the oxidative status of cysteine 177. This rapid reacting mechanism to transduce cellular redox state to a conformational change like a clear "on-off switch" suggests that HP1γ is a functional redox sensor.

During the cellular response to oxidative stress, an increase in oxidants can trigger alterations in transcription levels through direct activation or by promoting a change in the subcellular localization of transcription factors by oxidizing reactive cysteine residues (25). Among these oxidative responses, the disulfide dimerization of HP1γ demonstrated in this study appears to be one of the most rapid transcriptional regulatory mechanisms. TIF1β is a universal co-repressor for the Krüppel-associated box domain containing the zinc finger protein (KRAB-ZNF) family of transcription factors, and it is the major protein binding the CSD of HP1 (28–31). TIF1β also works as a scaffold for the repressor complex, and its interaction with HP1 is essential for its repression activity (12, 39–41). Recent findings have revealed that the binding of HP1 to TIF1β is essential for their coordinated function on the promoter of the endogenous genes (42). Therefore, the reversing effect for the repressive ability of TIF1β caused by HP1γ disulfide dimerization might be required for a short period of adaptation against oxidative stress. Downstream genes regulated by these scaffold complexes remain to be clarified in the future analysis.

In conclusion, our study suggests that HP1 potentially acts as a rapid redox sensor, and it may connect the intracellular redox state with transcriptional regulation under various physiological conditions.

Acknowledgments—We thank David C. Schultz and Takahiro Nagase for the plasmid constructs. We thank Saori Ikezawa and Yoko Hamada for technical assistance and Yasunori Shintani for thoughtful discussions.

REFERENCES

1. James, T. C., and Elgin, S. C. (1986) *Mol. Cell. Biol.* **6,** 3862–3872
2. Wallrath, L. L. (1998) *Curr. Opin. Genet. Dev.* **8,** 147–153
3. Bannister, A. J., Zegerman, P., Partridge, J. F., Miska, E. A., Thomas, J. O., Allshire, R. C., and Kouzarides, T. (2001) *Nature* **410,** 120–124
4. Nakayama, J., Rice, J. C., Strahl, B. D., Allis, C. D., and Grewal, S. I. (2001) *Science* **292,** 110–113
5. Lachner, M., O'Carroll, D., Rea, S., Mechtler, K., and Jenuwein, T. (2001) *Nature* **410,** 116–120
6. Brasher, S. V., Smith, B. O., Fogh, R. H., Nietlispach, D., Thiru, A., Nielsen, P. R., Broadhurst, R. W., Ball, L. J., Murzina, N. V., and Laue, E. D. (2000) *EMBO J.* **19,** 1587–1597
7. Thiru, A., Nietlispach, D., Mott, H. R., Okuwaki, M., Lyon, D., Nielsen, P. R., Hirshberg, M., Verreault, A., Murzina, N. V., and Laue, E. D. (2004) *EMBO J.* **23,** 489–499
8. Grewal, S. I., and Jia, S. (2007) *Nat. Rev. Genet.* **8,** 35–46
9. Lomberk, G., Wallrath, L., and Urrutia, R. (2006) *Genome Biol.* **7,** 228
10. Schultz, D. C., Ayyanathan, K., Negorev, D., Maul, G. G., and Rauscher, F. J., 3rd. (2002) *Genes Dev.* **16,** 919–932
11. Maison, C., and Almouzni, G. (2004) *Nat. Rev. Mol. Cell Biol.* **5,** 296–304
12. Sripathy, S. P., Stevens, J., and Schultz, D. C. (2006) *Mol. Cell. Biol.* **26,** 8623–8638
13. Cammas, F., Janoshazi, A., Lerouge, T., and Losson, R. (2007) *Differentiation* **75,** 627–637
14. Filesi, I., Cardinale, A., van der Sar, S., Cowell, I. G., Singh, P. B., and Biocca, S. (2002) *J. Cell Sci.* **115,** 1803–1813
15. Nielsen, A. L., Sanchez, C., Ichinose, H., Cerviño, M., Lerouge, T., Chambon, P., and Losson, R. (2002) *EMBO J.* **21,** 5797–5806
16. Vassallo, M. F., and Tanese, N. (2002) *Proc. Natl. Acad. Sci. U.S.A.* **99,** 5919–5924
17. Lomberk, G., Bensi, D., Fernandez-Zapico, M. E., and Urrutia, R. (2006) *Nat. Cell Biol.* **8,** 407–415
18. Gilbert, N., Boyle, S., Sutherland, H., de Las Heras, J., Allan, J., Jenuwein, T., and Bickmore, W. A. (2003) *EMBO J.* **22,** 5540–5550
19. Ritou, E., Bai, M., and Georgatos, S. D. (2007) *J. Cell Sci.* **120,** 3425–3435
20. Mateescu, B., Bourachot, B., Rachez, C., Ogryzko, V., and Muchardt, C. (2008) *EMBO Rep.* **9,** 267–272
21. Vakoc, C. R., Mandat, S. A., Olenchock, B. A., and Blobel, G. A. (2005) *Mol. Cell* **19,** 381–391
22. Ayoub, N., Jeyasekharan, A. D., Bernal, J. A., and Venkitaraman, A. R. (2008) *Nature* **453,** 682–686
23. Petta, T. B., Nakajima, S., Zlatanou, A., Despras, E., Couve-Privat, S., Ishchenko, A., Sarasin, A., Yasui, A., and Kannouche, P. (2008) *EMBO J.* **27,** 2883–2895
24. Asano, Y., Takashima, S., Asakura, M., Shintani, Y., Liao, Y., Minamino, T., Asanuma, H., Sanada, S., Kim, J., Ogai, A., Fukushima, T., Oikawa, Y., Okazaki, Y., Kaneda, Y., Sato, M., Miyazaki, J., Kitamura, S., Tomoike, H., Kitakaze, M., and Hori, M. (2004) *Nat. Genet.* **36,** 123–130
25. D'Autréaux, B., and Toledano, M. B. (2007) *Nat. Rev. Mol. Cell Biol.* **8,** 813–824
26. Oka, S., Ohno, M., Tsuchimoto, D., Sakumi, K., Furuichi, M., and Nakabeppu, Y. (2008) *EMBO J.* **27,** 421–432
27. Cowieson, N. P., Partridge, J. F., Allshire, R. C., and McLaughlin, P. J. (2000) *Curr. Biol.* **10,** 517–525
28. Friedman, J. R., Fredericks, W. J., Jensen, D. E., Speicher, D. W., Huang, X. P., Neilson, E. G., and Rauscher, F. J., 3rd. (1996) *Genes Dev.* **10,** 2067–2078
29. Kim, S. S., Chen, Y. M., O'Leary, E., Witzgall, R., Vidal, M., and Bonventre, J. V. (1996) *Proc. Natl. Acad. Sci. U.S.A.* **93,** 15299–15304
30. Le Douarin, B., Nielsen, A. L., Garnier, J. M., Ichinose, H., Jeanmougin, F., Losson, R., and Chambon, P. (1996) *EMBO J.* **15,** 6701–6715
31. Moosmann, P., Georgiev, O., Le Douarin, B., Bourquin, J. P., and Schaffner, W. (1996) *Nucleic Acids Res.* **24,** 4859–4867
32. Itokawa, Y., Yanagawa, T., Yamakawa, H., Watanabe, N., Koga, H., and Nagase, T. (2009) *Biochem. Biophys. Res. Commun.* **388,** 689–694
33. Koike, N., Maita, H., Taira, T., Ariga, H., and Iguchi-Ariga, S. M. (2000) *FEBS Lett.* **467,** 17–21
34. Zhao, T., Heyduk, T., and Eissenberg, J. C. (2001) *J. Biol. Chem.* **276,** 9512–9518
35. Badugu, R., Yoo, Y., Singh, P. B., and Kellum, R. (2005) *Chromosoma* **113,** 370–384
36. Leroy, G., Weston, J. T., Zee, B. M., Young, N. L., Plazas-Mayorca, M. D., and Garcia, B. A. (2009) *Mol. Cell. Proteomics* **8,** 2432–2442
37. Wang, G., Ma, A., Chow, C. M., Horsley, D., Brown, N. R., Cowell, I. G., and Singh, P. B. (2000) *Mol. Cell. Biol.* **20,** 6970–6983
38. Nielsen, A. L., Oulad-Abdelghani, M., Ortiz, J. A., Remboutsika, E., Chambon, P., and Losson, R. (2001) *Mol. Cell* **7,** 729–739
39. Nielsen, A. L., Ortiz, J. A., You, J., Oulad-Abdelghani, M., Khechumian, R., Gansmuller, A., Chambon, P., and Losson, R. (1999) *EMBO J.* **18,** 6385–6395
40. Ayyanathan, K., Lechner, M. S., Bell, P., Maul, G. G., Schultz, D. C., Yamada, Y., Tanaka, K., Torigoe, K., and Rauscher, F. J., 3rd. (2003) *Genes Dev.* **17,** 1855–1869
41. Smallwood, A., Black, J. C., Tanese, N., Pradhan, S., and Carey, M. (2008) *Nat. Struct. Mol. Biol.* **15,** 318–320
42. Riclet, R., Chendeb, M., Vonesch, J. L., Koczan, D., Thiesen, H. J., Losson, R., and Cammas, F. (2009) *Mol. Biol. Cell* **20,** 296–305
43. Moreland, J. L., Gramada, A., Buzko, O. V., Zhang, Q., and Bourne, P. E. (2005) *BMC Bioinformatics* **6,** 21

This Review is part of a thematic series on **Endoplasmic Reticulum Stress and Cardiac Diseases**, which includes the following articles:
What Is the Role of ER Stress in the Heart? Introduction and Series Overview [*Circ Res.* 2010;107:15–18]
The Role of Endoplasmic Reticulum Stress in the Progression of Atherosclerosis [*Circ Res.* 2010;107:839–850]

Endoplasmic Reticulum Stress As a Therapeutic Target in Cardiovascular Disease

Biology of Endoplasmic Reticulum Stress in the Heart
Interrelationship Between Cardiac Hypertrophy, Heart Failure, and Chronic Kidney Disease—Endoplasmic Reticulum

Masafumi Kitakaze, Guest Editor

Endoplasmic Reticulum Stress As a Therapeutic Target in Cardiovascular Disease

Tetsuo Minamino, Issei Komuro, Masafumi Kitakaze

Abstract: **Cardiovascular disease constitutes a major and increasing health burden in developed countries. Although treatments have progressed, the development of novel treatments for patients with cardiovascular diseases remains a major research goal. The endoplasmic reticulum (ER) is the cellular organelle in which protein folding, calcium homeostasis, and lipid biosynthesis occur. Stimuli such as oxidative stress, ischemic insult, disturbances in calcium homeostasis, and enhanced expression of normal and/or folding-defective proteins lead to the accumulation of unfolded proteins, a condition referred to as ER stress. ER stress triggers the unfolded protein response (UPR) to maintain ER homeostasis. The UPR involves a group of signal transduction pathways that ameliorate the accumulation of unfolded protein by increasing ER-resident chaperones, inhibiting protein translation and accelerating the degradation of unfolded proteins. The UPR is initially an adaptive response but, if unresolved, can lead to apoptotic cell death. Thus, the ER is now recognized as an important organelle in deciding cell life and death. There is compelling evidence that the adaptive and proapoptotic pathways of UPR play fundamental roles in the development and progression of cardiovascular diseases, including heart failure, ischemic heart diseases, and atherosclerosis. Thus, therapeutic interventions that target molecules of the UPR component and reduce ER stress will be promising strategies to treat cardiovascular diseases. In this review, we summarize the recent progress in understanding UPR signaling in cardiovascular disease and its related therapeutic potential. Future studies may clarify the most promising molecules to be investigated as targets for cardiovascular diseases. (*Circ Res.* 2010;107:1071-1082.)**

Key Words: heart failure ■ ischemic heart diseases ■ atherosclerosis ■ ER stress ■ unfolded protein response

Although the clinical management of heart failure has advanced substantially,[1] and prevention strategies for atherosclerosis focused on managing the established risk factors have progressed markedly,[2] cardiovascular disease still constitutes a major and increasing health burden in developed countries. Thus, the development of novel treatments for patients with cardiovascular diseases remains a major research priority.

The endoplasmic reticulum (ER) comprises a complex membranous network found in all eukaryotic cells. It plays a crucial role in the folding of secretory and membrane proteins, calcium homeostasis, and lipid biosynthesis.[3–5] ER

Original received July 6, 2010; revision received September 10, 2010; accepted September 14, 2010. In August 2010, the average time from submission to first decision for all original research papers submitted to *Circulation Research* was 13.2 days.

From the Department of Cardiovascular Medicine (T.M., I.K.), Osaka University Graduate School of Medicine; and Department of Cardiovascular Medicine (M.K.), National Cerebral and Cardiovascular Center Hospital, Japan.

This manuscript was sent to Ali J. Marian, Consulting Editor, for review by expert referees, editorial decision, and final disposition.

Correspondence to Tetsuo Minamino, MD, PhD, Department of Cardiovascular Medicine, Osaka University Graduate School of Medicine, 2-2 Yamadaoka, Suita, Osaka 565-0871, Japan. E-mail minamino@cardiology.med.osaka-u.ac.jp

Circulation Research **is available at http://circres.ahajournals.org** **DOI: 10.1161/CIRCRESAHA.110.227819**

Non-standard Abbreviations and Acronyms

AMPK	AMP-activated protein kinase
ASK1	apoptosis signal-regulating kinase 1
ATF	activating transcription factor
Bcl-2	B-cell lymphoma 2
CHOP	CCAAT/enhancer binding protein (C/EBP) homologous protein
CREBH	cAMP response element-binding protein H
eIF2α	eukaryotic initiation factor-2α
ER	endoplasmic reticulum
ERAD	endoplasmic reticulum–associated degradation
ERO1	endoplasmic reticulum oxidoreductin 1
GRP78	glucose-regulated protein 78 kDa
IκB	inhibitor of κB
I/R	ischemia/reperfusion
IRE1	inositol-requiring protein 1
JNK	c-Jun N-terminal kinase
KO	knockout
MANF	mesencephalic astrocyte-derived neurotrophic factor
PARM-1	prostatic androgen repressed message-1
PBA	phenylbutyrate
PDI	protein disulfide isomerase
PERK	protein kinase–like endoplasmic reticulum kinase
PKA	protein kinase A
ROS	reactive oxygen species
SERCA	sarcoplasmic reticulum calcium-transporting ATPase
TNF	tumor necrosis factor
TRAF2	tumor necrosis factor receptor–associated factor 2
TRB3	tribbles 3
TLR	Toll-like receptor
UPR	unfolded protein response
XBP1	X box–binding protein-1

stress that disrupts ER function can occur in response to a wide variety of cellular stressors that lead to the accumulation of unfolded and misfolded proteins in the ER. Initially, ER transmembrane sensors detect the accumulation of unfolded proteins and activate transcriptional and translational pathways that deal with unfolded and misfolded proteins, known as the unfolded protein response (UPR). However, the failure to relieve prolonged or severe ER stress causes the cell to undergo apoptotic cell death. Recently, adaptive and proapoptotic pathways of UPR have been implicated in the pathophysiology of human diseases, including cardiovascular diseases, neurodegenerative diseases, diabetes mellitus, obesity, and liver diseases.[3–5] In this review, we summarize the molecular mechanisms of UPR in cardiovascular diseases and possible therapeutic interventions targeting the components involved in the UPR.

Endoplasmic Reticulum

The ER is the cellular organelle for the synthesis and folding of secreted and membrane-bound proteins and the first site of the secretory pathway.[3–5] Approximately one-third of newly synthesized proteins are translocated into the ER, where they fold and assemble with the assistance of ER chaperones and oxidoreductases.[6] The ER lumen constitutes a specialized environment for proper protein folding and assembly.[3–5] For instance, the ER contains the millimolar concentrations of free calcium within the cell. Glucose-regulated protein 78 kDa (GRP78), which is the ER-located member of the family of heat shock protein 70 molecular chaperones, promotes the folding of hydrophobic regions in polypeptides to the interior in a calcium-dependent manner.[7] The oxidizing environment in the ER is crucial for the formation of disulfide bonds mediated by protein disulfide isomerase (PDI) and ER oxidoreductin (ERO)1, which serves as the terminal electron acceptor with oxygen.[8] Reactive oxygen species (ROS) generated as a product of disulfide bond formation in the ER cause oxidative stress and contribute to apoptotic cell death.[9] As a consequence of this special environment, the ER is highly sensitive to stresses that deplete its ATP or calcium and alter the intraluminal redox status.

Adaptive and Proapoptotic Pathways of UPR

When unfolded proteins accumulate in the ER, 3 ER transmembrane sensors detect them to initiate 3 distinct UPR branches mediated by the following molecules: protein kinase-like ER kinase (PERK), the inositol requiring kinase (IRE)1, and the transcription factor-activating transcription factor (ATF)6 (Figure 1).[3–5,10] These UPR sensors have N termini in the lumen of the ER and C termini in the cytosol, thereby connecting the ER and cytosol. All 3 sensors have luminal domains that bind to the ER chaperone GRP78 under normal, unstressed conditions.[11] However, on ER stress, GRP78 is released from these sensors, permitting their oligomerization and thereby initiating the UPR to deal with accumulated unfolded proteins. However, if the ER stress is prolonged and/or severe, the ER initiates apoptotic cell death signaling.[12] ER sensor proteins including PERK and IRE1 are responsible for both the adaptive and the proapoptotic pathways of UPR.[12]

IRE1α is the most fundamental ER stress sensor and is conserved from yeast to humans. On ER stress, the dimerization and autophosphorylation of IRE1 elicit an endoribonuclease activity that specifically cleaves the mRNA encoding the transcription factor X-box binding protein (XBP)1.[3–5] This unconventional splicing reaction is required for the translation of transcriptionally active XBP1. Active (spliced) XBP1 binds to the ER stress response element in the promoters of a wide variety of UPR-target genes whose products help to fold and degrade the proteins.[3–5] Our recent study demonstrated that spliced XBP1 can regulate the expression of brain natriuretic peptide (BNP), a non–UPR-target gene, through a novel AP1/CRE-like element in cardiomyocytes.[13] Interestingly, p85α, the regulatory subunit of phosphatidylinositol 3-kinase (PI3K), was found to interact with XBP1 and increase the nuclear translocation of XBP1.[14] In ob/ob mice, the interaction between them is lost, resulting in a severe defect in both the translocation of XBP1 and the resolution of ER stress.[14] These findings suggest that non-UPR and UPR genes are regulated by spliced XBP1.

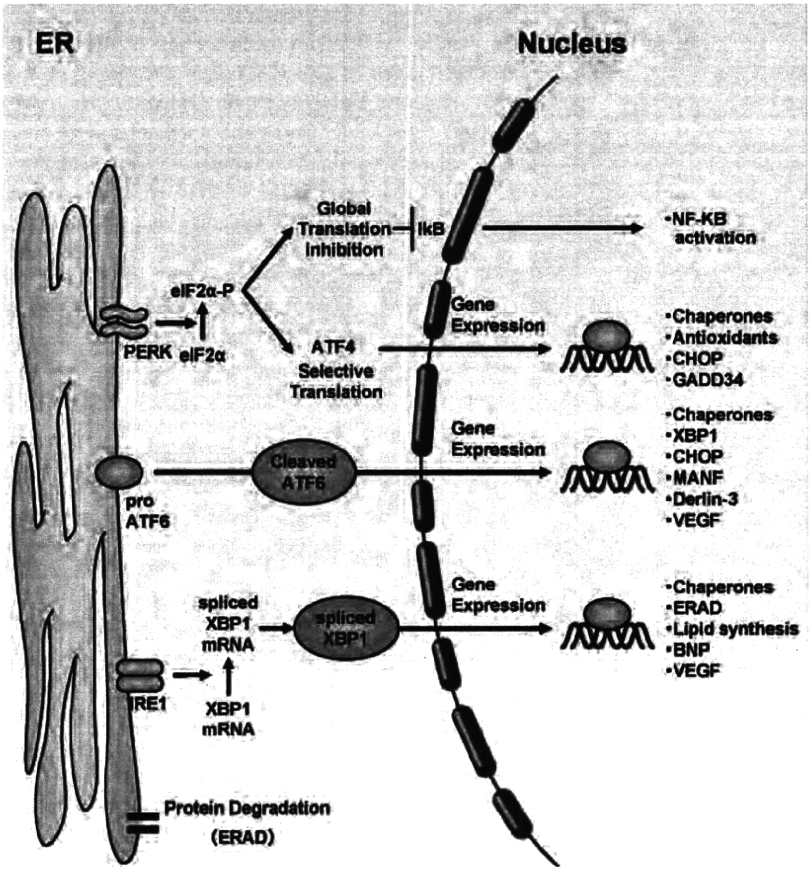

Figure 1. UPR pathways. On ER stress, GRP78 dissociates from 3 ER transmembrane sensors including PERK, IRE1, and ATF6, allowing their activation. PERK phosphorylates eIF2α, which is dephosphorylated by GADD34, consequently shutting off protein translation. However, paradoxically, eIF2α phosphorylation induces the selective translation of a transcriptional factor ATF4 to induce the UPR-target genes. ATF6 translocates from ER to Golgi, in which ATF6 cleavage produces a transcriptionally active cytosolic fragment. ATF6 activates a subset of UPR- and non–UPR-target genes, including XBP1. On ER stress, activation of IRE1 elicits an endoribonuclease activity that specifically cleaves the mRNA encoding the transcriptional factor XBP1. This unconventional splicing reaction is required for translation of transcriptionally active XBP1 to induce UPR- and non–UPR-target genes.

In addition to endoribonuclease activity, IRE1α mediates cell death and inflammatory signaling (Figure 2). IRE1α interacts with the adaptor protein tumor necrosis factor TNF receptor–associated factor (TRAF) 2, which leads to the activation of a mitogen-activated protein kinase kinase kinase, apoptosis signal-regulating kinase (ASK)1[15,16] and caspase 12.[17,18] The ASK1 pathway contributes to the pathogenesis of heart and neurodegenerative diseases.[19,20] Furthermore, IRE1α/TRAF2 can also recruit the inhibitor of κB (IκB) kinase, which mediates the activation of nuclear factor κB, suggesting that IRE1α might provide a link between ER stress and inflammation.[21]

PERK is another ER stress sensor and a serine threonine kinase that phosphorylates eukaryotic translation initiation factor (eIF)2α on ER stress, resulting in the inhibition of most cap-dependent translation, which requires the interaction of certain key molecules with a special tag bound to the 5′-end of mRNA, termed a cap.[3–5] One example is the translational inhibition of IκB, resulting in the activation of nuclear factor κB.[22] However, paradoxically, several mRNAs require the phosphorylation of eIF2α for their translation. One example is the mRNA encoding ATF4, a transcriptional factor that binds to the promoter of the gene encoding GADD34, the regulatory subunit of the phosphatase that dephosphorylates eIF2α and restores cap-dependent translation.[23] CCAAT/enhancer-binding protein homologous protein (CHOP) is the proapoptotic basic-leucine zipper transcription factor that is regulated by the ATF4 and ATF6 pathways.[3–5] The deletion of the CHOP gene protects against cell death induced by a pharmacological ER stressor, mechanical stretching and pathophysiological stimuli, such as ischemia and pressure overload.[24–28] Although the potential mechanisms by which CHOP induces cell death are not well identified, one important pathway by which CHOP induces cell apoptosis is regulation of the balance of proapoptotic and antiapoptotic B-cell lymphoma (Bcl)-2 family proteins. CHOP represses the expression of antiapoptotic proteins Bcl-2 and Bnip3 in cardiomyocytes.[27,29] In addition, CHOP mediates the direct transcriptional induction and translocation to the ER membrane of Bim, a proapoptotic BH3-only protein of the Bcl-2 protein family, in conditions of ER stress.[30]

The third ER stress member is ATF6, a transmembrane basic leucine zipper transcription factor.[3–5] ER stress induces the release of GRP78 from ATF6 and permits ATF6 translocation from the ER to the Golgi, where S1P- and S2P-mediated proteolytic cleavage produces a transcriptionally active cytosolic fragment. Cleaved ATF6 binds to the ER stress response element in the promoters of UPR target genes, including XBP1. Recently, several ATF6-related proteins with distinct tissue distributions were identified.[31,32] Interestingly, lipopolysaccharide and cytokines activate cAMP response element-binding protein (CREB)H, which is a hepatocyte-specific ER-anchored transcription factor that activates a subset of genes associated with inflammation but

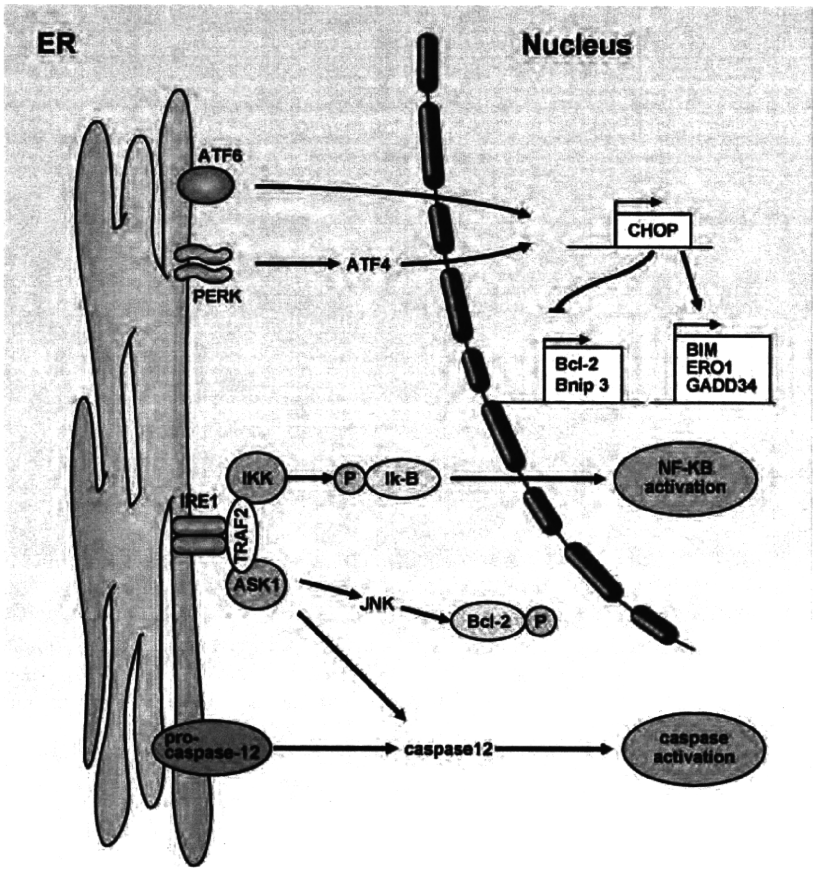

Figure 2. Proapoptotic pathways of UPR. CHOP is the proapoptotic bZIP transcription factor that is regulated mainly by ATF4- and ATF6-dependent pathways. CHOP represses the expression of the antiapoptotic proteins Bcl-2 and Bnip3. In addition, CHOP mediates the direct transcriptional induction and translocation to the ER membrane of Bim, a proapoptotic BH3-only protein of the Bcl-2 family, on ER stress. IRE1α interacts with the adaptor protein TRAF2. The IRE1α/TRAF2 complex interacts with ASK1, which subsequently phosphorylates JNK. Activation of JNK induces apoptotic cell death through the phosphorylation of several Bcl-2 family members. The IRE1α/TRAF2 complex also interacts with IκB kinase, which leads to nuclear factor κB (NF-κB) activation. On ER stress, procaspase 12 is cleaved and activated, which in turn activates caspase-9/3, thereby leading to mitochondria-independent cell death.

not UPR.[31] These findings suggest that CREBH integrates the UPR with the acute phase response. PARM-1 (prostatic androgen repressed message 1) was shown to be induced in a cardiac hypertrophy and subsequent heart failure model.[33] PARM-1 expression is induced by ER stress, which plays a protective role in cardiomyocytes through the regulation of PERK, ATF6 and CHOP expression. The existence of tissue-specific UPR components allows for the response to tissue-specific stress.

Misfolded ER proteins are exported from the ER into the cytosol by a process termed ER-associated protein degradation (ERAD) or retrotranslocation.[3,34] Most ERAD substrates are ubiquitinated and extracted by a cytosolic ATPase named p97 before degradation by the proteasome. Defects in ERAD cause the accumulation of misfolded proteins in the ER and thus trigger the UPR.[35]

ER Stress and Cardiovascular Diseases

Experimentally, the ER environment can be perturbed by substances such as dithiothreitol, thapsigargin, or tunicamycin, which alter the redox status, calcium levels and protein glycosylation in the ER, respectively.[36] When cells are treated with one of these compounds, ER protein folding is impaired, and the accumulation of unfolded proteins activates the adaptive and proapoptotic pathways of the UPR.[3–5]

Pathophysiological stimuli also activate UPR. Hypoxia, angiotensin II and tumor necrosis factor (TNF)-α activate adaptive and proapoptotic pathways of the UPR in cultured cardiomyocytes.[37–39] The cardiac-specific deposition of aggregated β-amyloid[40] or polyglutamine preamyloid oligomer[41] activated the component of UPR in mouse transgenic hearts. Cyclic stretching significantly increases CHOP protein in cultured cardiomyocytes,[28] and CHOP expression increases in pressure-overloaded hearts.[38] Metabolic factors such as cholesterol, homocysteine, glucose, fatty acid, and palmitate can also trigger ER stress.[42,43] These findings suggest that activation of UPR by pathophysiological stimuli is involved in the development of cardiovascular diseases.

Cardiac Hypertrophy and Failure

Electron microscopic analyses have revealed that the proliferation of tubules of the ER is a common finding in degenerated cardiomyocytes, suggesting that the ER is overloaded in this condition.[44] Oxidative stress, hypoxia, and enhanced protein synthesis found in failing hearts potentially enhance ER stress. Indeed, in patients with heart failure, we and others have shown the existence of spliced XBP1 and markedly increased GRP78 expression, suggesting that UPR activation is associated with the pathophysiology of heart failure in humans.[13,38,45] Our study also showed that mRNA levels of ATF4 and CHOP are increased in these patients.[27] Furthermore, ubiquitinated proteins are accumulated in human failing hearts.[46,47] These findings suggest that protein quality control is impaired in human failing hearts.

In Dahl salt–sensitive rats, a high-salt diet leads to hypertension, cardiac hypertrophy, and subsequent heart failure, as well as significant increases in both GRP78 and CHOP expression.[33] Consistent with these findings, in mice that received transaortic constriction, GRP78 and CHOP are upregulated.[38] Interestingly, UPR activation has been found in both hypertrophic and failing hearts, whereas the activation of ER-initiated apoptosis CHOP, but not c-Jun N-terminal kinase (JNK) or caspase 12, is found only in failing hearts.[38] These findings suggest that UPR activation is consistently found in hearts subjected to pressure overload. However, when the ER stress is prolonged, the ER-initiated apoptosis signal CHOP is activated in failing mouse hearts induced by pressure overload. To clarify the role of CHOP in hypertrophic and subsequently failing hearts by pressure overload, we performed transaortic constriction using CHOP knockout (KO) mice.[27] We observed that both cardiac hypertrophy and dysfunction were attenuated in CHOP KO mice compared with wild type. In CHOP KO mice, the enhanced phosphorylation of eIF2α, which was attributable to the lack of negative regulation by GADD34, may lead to the global repression of translation. This may explain the mechanism by which cardiac hypertrophy is reduced in pressure-overloaded hearts of CHOP KO mice. Furthermore, microarray analysis revealed that CHOP positively and negatively regulates several proapoptotic and antiapoptotic molecules of the Bcl-2 family. These findings suggest that CHOP might be a promising molecular target for the treatment of cardiac hypertrophy and failure.

Protein accumulation resulting from the impairment of the secretory pathway or mutant protein synthesis also causes heart failure. In transgenic mice systemically expressing a mutant KDEL (Lys-Asp-Glu-Leu) receptor,[48] which is a retrieval receptor for ER chaperones in the early secretory pathway, disturbed recycling of misfolded proteins between the ER and Golgi complex and enhanced expression of CHOP and apoptosis were observed in the mutant hearts. The transgenic mice exhibited dilated cardiomyopathy without obvious findings in other tissues, suggesting that the heart is sensitive to ER stress. The transgenic expression of mutant proteins in neural and cardiac tissues is a good model to test whether intracellular aggregation affects cardiac function.[40,41,49,50]

Viruses exploit the translational machinery of the host cell to synthesize their viral proteins, leading to increased folding pressure on the ER and chaperone upregulation.[51,52] Thus, it is likely that the adaptive and proapoptotic pathways of UPR are involved in the pathophysiology of viral myocarditis. Furthermore, Mao et al demonstrated that ER stress plays an important role in cardiomyocyte apoptosis and the development of dilated cardiomyopathy in rabbits immunized with a peptide corresponding to the β1-aderenoceptor.[53,54] These findings suggest that the UPR plays an important role in the pathophysiology of virus and autoimmune heart diseases.

Ischemic Heart Diseases

In a myocardium that has experienced ischemia/reperfusion (I/R), myocardial death and severe inflammation are induced because of the depletion of oxygen and nutrients, followed by the sudden burden of oxygen free radicals and production of proinflammatory cytokines.[55] Either of these stimuli can potentially induce the adaptive and proapoptotic pathways of UPR. Indeed, increased expression of UPR-related genes is reported in cardiomyocytes near myocardial infarction in mice and humans.[56–58]

Martindale et al demonstrated the role of ATF6, a component of the UPR, in I/R injury using transgenic mice with cardiac-restricted expression of a novel tamoxifen-activated form of ATF6.[59] The tamoxifen-treated transgenic mouse hearts exhibit better functional recovery from ex vivo I/R, as well as significantly reduced necrosis and apoptosis and increased expression of ER-resident chaperones GRP78 and -94. Toko et al demonstrated that the treatment of mice with 4-(2-aminoethyl) benzenesulfonyl fluoride, an inhibitor of ATF6, further reduces cardiac function and increases the mortality rate after myocardial infarction.[58] These findings suggest that ATF6 exerts cardioprotective effects on I/R injury. Furthermore, Glembotski and colleagues showed that ATF6 activation induces numerous genes in cultured cardiomyocytes, including MANF (mesencephalic astrocyte-derived neurotrophic factor).[60] Knockdown of endogenous MANF with microRNA increases cell death on simulated I/R, whereas the addition of recombinant MANF to media protected the cultured cardiac myocytes from simulated I/R-mediated death.[60] It was also shown that activated ATF6 induces the Derlin-3 gene, which encodes an important component of the ERAD machinery. Overexpression of Derlin-3 enhances ERAD and protects cardiomyocytes from simulated ischemia-induced cell death.[61]

In rat neonatal cultured cardiomyocytes, hypoxia increased XBP1 mRNA splicing and GRP78 protein levels.[56] Because infection with a recombinant adenovirus encoding dominant-negative XBP1 augments hypoxia/reoxygenation-induced apoptosis, the XBP1 arm of the UPR may play cardioprotective roles against hypoxic insult. Vitadello et al demonstrated that the overexpression of GRP94, the expression of which is regulated by XBP1 and ATF6, reduces myocyte necrosis caused by calcium overload or simulated ischemia in cardiac H9C2 muscle cells.[62] In addition, it was reported that ischemic preconditioning or postconditioning reduces cardiac damage associated with UPR activation.[63,64] In human heart samples, Severino et al demonstrated that PDI is upregulated 3-fold in the viable periinfarct myocardial region.[65] Adenoviral-mediated PDI gene transfer to the mouse heart results in a 2.5-fold smaller infarct size and significantly reduces cardiomyocyte apoptosis in the periinfarct region and the smaller left ventricular end-diastolic diameter compared with treatment with a transgene-null adenoviral vector.

On the other hand, Terai et al demonstrated that hypoxia induces CHOP expression and the cleavage of caspase 12; this effect is significantly inhibited by pretreatment with a pharmacological activator of AMP-activated protein kinase (AMPK).[37] This finding indicates that the proapoptotic pathways of the UPR are involved in cell death by hypoxic stimuli. In addition, Nickson et al demonstrated that ER stress induces the expression of PUMA, a proapoptotic member of the BCL-2 family, and that the suppression of PUMA expression leads to inhibition of cardiomyocyte apoptosis